STRUCTURAL AND FUNCTIONAL CHARACTERIZATION OF THE *ESCHERICHIA COLI* METNI METHIONINE TRANSPORTER

Thesis by

Phong Thanh Nguyen

In Partial Fulfillment of the Requirements for the

degree of

Doctor of Philosophy

CALIFORNIA INSTITUTE OF TECHNOLOGY

Pasadena, California

2018

(Defended January 19, 2018)

Phong Thanh Nguyen

ORCID: 0000-0002-6390-7350

This work is dedicated to three Caltech professors,

Prof. Pamela Bjorkman

Prof. Doug Rees

Prof. Kai Zinn,

who saved my scientific career before it even started.

ACKNOWLEDGMENTS

I would like to express my deepest gratitude to my advisor, Prof. Doug Rees, who has given me a tremendous amount of support throughout the years. He has turned me from an average student into an independent and passionate scientist who is willing to take on a big challenge and pursue it until the end. I remember that whenever I felt doubt about my project, I would set up a meeting with him, and sure enough I never left any meeting without my mind energized and excited for the next trials.

I would also like to thank my committee members, Profs Jack Beauchamp, Shu-ou Shan, and Bil Clemons. Their advice guided me to the finish line of my project. Prof. Beauchamp and Prof. Shan always made sure that I was going on the right track. I thank Prof. Clemons for his inspiring words to me, "you should publish something that advances the field," which made me really think about why I'm a scientist.

Special thanks to team MetNI, past and present, Dr. Eric Johnson, and Dr. Janet Yang for teaching me how to work with membrane proteins; Dr. Li Qiwen for helping me determine some binding constants; Jeff Lai and Allen Lee for being my two amazing partners who have been working with me in this project for the longest time; Dr. Naima Sharaf for teaching me Illustrator and Overleaf; Christopher Muller and Kyle Lopez, two visiting students who joined forces with me in tackling the MetNI project during their visits.

Dr. Jens Kaiser and Chengcheng Fan are my favorite people with whom I often discuss X-ray crystallography. Many thanks to Dr. Kaiser for helping with crystal shipping, data collection, and troubleshooting for structural determination throughout the years.

And of course, thanks to our excellent administrative assistant, Phoebe Ray, and the rest of the Rees group for making a friendly atmosphere and collaborative environment.

I thank Stefan Petrovic, Sara Weaver, and Haoqing Wang, who offer their valuable knowledge to help with my experimental issues, as well as Dr. Nathan Dalleska for his ICP-MS instrumental training.

As an international student who studied abroad for the first time, I thought I would be suffering so much from cultural shock; but I was lucky enough to be surrounded by amazing, true friends who help me deal with struggles. In one way or another, Limei Zhang and Gabriele Meloni have become my mentors in science and life. I learned so much from their scientific ethics and how they balance their life for friends, families, and work. They are surely my role models. Thanks, Limei, for always reminding me that "failure is not an option". Raymond and Nadia became a part of my family. Ray was probably the first person who I met at Caltech. He has been the one who revised every single document that I composed for funding applications and other things. Thank you Ray and Nadia for sharing an amazing adventure to Alaska with me and my wife. I can't wait to share with you one of your happiest moments in life, your wedding, this summer.

I'm so thankful for great friendships I have with Aron Kamajaya, Monica Lui, Feng Chen, Dina Malouda, and Yong-Jun Lin. Those "Costco Fridays" really bonded us together. Aron and I became close friends after class. Although we did homework together, we never violated the "honor code" (proof: he always got an A while I barely did). Our group also had so many fun activities, such as playing PS4, going to church, and meeting every single weekend, which gave me no time left to experience culture shock.

Thanks to Renee Arias and Keith Beadle, Belinda Wenke and Andy Buller, Kathryn Perez and Thomas Spatzal, for their great friendships.

It has been so much fun to participate in the Vietnamese Student Association, where I met my Vietnamese comrades who share with me so many values of Vietnamese students. We have been having so much fun with hiking/camping trips, parties, and celebrations. We always look out and help each other to overcome difficult moments.

It was a great pleasure to be a part of the Caltech badminton club, where I learnt leadership and built friendship with great friends, including Remy Mevel and Sophia Dai, Mayank Raj, Yi Cao, Juliette Xiong, and others.

I would like to thank my families for their support. I thank my parent-in-law, and sister- and brother-in-law, who have incorporated me into their lives. I thank my mom for her unconditional love, and my dad for being hard to me so that I learned the value of education when I grew up. Although during my childhood my family was quite poor, my dad always told me that he wouldn't buy me anything but books, and any book that I wanted.

Duong (Amy) Nguyen is my wife and my best friend. We first met at Zuckerberg's house, i.e. on Facebook, six years ago. It was a "love at the first sight" for me. We decided to get married only a month after we first met in person, and I knew it was my best decision ever. We have been enjoying happy moments together every day. I'm looking forward to new adventures with her and with our children in the future.

Viet Anh (Vian), our 4-month-old son, is the best “crystal” that Amy and I have ever grown together. We cherish every second with him. He has really been my lucky charm, and gave me so much mental support that carried me throughout the hardest time of my PhD work. Because of him, I pushed myself to the limit to complete my project.

I would also like to thank my undergrad thesis advisors, Dr. Thuy H.A. Le and Dr. Hiep M. Dinh, for their early training. They really inspired me to learn, to love science, and to pursue the joys of discovering something new in science.

Finally, I will never forget a tipping point in my career a decade ago when I had a dream of studying abroad. Although I was not confident about myself (GPA: B^-), I was able to calm my nerves and tried submitting an application for a government scholarship in 2009. As an expected result, I was not one of the selected awardees. However, at the same time, I had an opportunity to interview with two professors at Caltech, Prof. Pamela Bjorkman and Prof. Kai Zinn, with whom I had the most exciting 1-hour conversation about science that I ever had in my life. They then promised to talk to the head of the funding program about my case. Consequently, the second list of awardees came out with my name on it. And I’m pretty sure that Pamela and Kai had to convince Doug to give an opportunity to an unknown average student like me. If it was not for Pamela, Kai, and Doug, I wouldn’t be able to study abroad, let alone study at Caltech. Because of that, everyday I told myself that I had to get it (my project) done so that they never felt regret for giving me that opportunity. This work is dedicated to them, the people who saved my career when it hadn’t even started.

And I would like to acknowledge the Vietnamese International Education Development grant for partially funding my tuition for the first two years of my PhD program.

ABSTRACT

Despite the ubiquitous role of ATP Binding Cassette (ABC) importers in nutrient uptake, only the *E. coli* maltose and vitamin B_{12} ABC transporters have been structurally characterized in multiple conformations relevant to the alternating access transport mechanism. To complement our previous structure determination of the *E. coli* MetNI methionine importer partner in the inward facing conformation (Kadaba et al. Science 321, 250-253, 2008), we have explored conditions stabilizing the outward facing conformation. Using two variants, the Walker B E166Q mutation with ATP and EDTA to stabilize MetNI in the ATP-bound conformation, and the N229A variant of the binding protein MetQ to disrupt methionine binding as shown in this work, a high affinity MetNIQ complex was formed with a dissociation constant measured to be 27 nM. We then solved a 2.95 Å resolution crystal structure of the outward-facing conformation of the MetNI transporter, in complex with its binding protein, MetQ. The structure sheds light on how the C-regulatory domains regulate transport activity by rearrangement of a hydrogen bonding network between their interfaces in two different conformations. Structure of the substrate-free homologous MetQ from *N. meningitides* was also resolved using the N-to-A mutation (N238A). Superimposition of the substrate-bound, substrate-free (homologous model) MetQ and the binding protein MetQ in complex with its MetNI transporter (complexed MetQ) reveals unexpected structural features of the complexed MetQ, indicates a different substrate delivery mechanism for the MetNI transporter. These structural insights, coupled with thermodynamic binding constant and *in vivo* transport studies, support an unconventional transport mechanism for the Type-I methionine ABC importer.

Key words: ABC transporter, methionine transporter, methionine-binding protein, MetNI, MetQ, L-methionine, transinhibition, outward-facing conformation

PUBLISHED CONTENT AND CONTRIBUTIONS

1. **Nguyen, P.T,** Lai, J.Y., Kaiser, J.T., Rees, D.C. "Structural basis for substrate stereo-specificity of the *Neisseria meningitides* MetQ methionine-binding protein." (in preparation)

P.T.N designed and conducted the experiments, and had primary responsibility for data analysis and manuscript preparation.

2. **Nguyen, P.T,** Lai, J.Y., Lee, A.T, Kaiser, J.T., Rees, D.C. "A dual role for the binding protein in methionine uptake by the MetNI ABC transporter." (submitted)

P.T.N designed and conducted the experiments, and had primary responsibility for data analysis and manuscript preparation.

3. **Nguyen, P.T**, Li, Q.W., Kadaba, N.S., Lai, J.Y., Yang J.G., Rees, D.C. "The contribution of methionine to the stability of the Escherichia coli MetNIQ ABC transporter-substrate binding protein complex." Biol Chem. 396(9–10), 1127–34. (2015). https://doi.org/10.1515/hsz-2015-0131

P.T.N participated in the experiments, data analysis and manuscript preparation.

4. Johnson, E., **Nguyen, P.T.**, Yeates, T.O., and Rees, D. C. "Inward Facing Conformations of the MetNI Methionine ABC Transporters: Implications for the Mechanism of Trans-inhibition." Protein Science 21, 84-96 (2012). https://doi.org/10.1002/pro.765

P.T.N participated in soaking experiments for the L-semethionine-bound MetNI structure (PDB:3TUZ) and manuscript preparation.

TABLE OF CONTENTS

Page

Acknowledgments iv

Abstract ix

Published content and contributions xi

Table of content xii

List of figures and tables xv

Nomenclature xvii

Chapter 1: Introduction 1

1.1.Introduction to ABC transporters and the *E. coli* methionine

ABC transporter 1

1.2.Background 1

1.3.Statement of problems 4

1.4.Primary research questions 5

1.5. Significance of study 5

1.6.Research Design 6

1.7.Outline of thesis 7

Bibliography 8

Chapter 2: The contribution of methionine to the stability of the *Escherichia coli*

MetNIQ ABC transporter- substrate binding protein complex 15

2.1. Introduction 15

2.2. Results and discussion 17

2.3. Materials and methods 26

2.3.1. Cloning, expression, and purification of MetQ 26

2.3.2. Purification of MetNI 27

2.3.3. MetQ crystallization and structure determination 27

2.3.4. Screening of substrate-binding deficient MetQ mutants 28

2.3.5. Qualitative determination of complex formation 30

2.3.6. Measurement of MetNIQ complex dissociation constant 30

Acknowledgment 33

Bibliography 33

Chapter 3: An unconventional mechanistic model for the *E. coli* type-I methionine ABC transporter 38

3.1. Introduction 38

3.2. Results and Discussion 40

3.2.1. Overall architectures of the MetNIQ complex in the outward-facing conformation 40

3.2.2. Unexpected features of MetQ in complex with MetNI indicating

new substrate delivery mechanism 44

3.2.3. Substrate cavity and gating mechanism 46

3.2.4. The effects of L-methionine to complex formation and stability of MetNIQ complex 49

3.2.5. Functional characterization of the MetNI methionine transporter confirms new roles of the binding protein MetQ 51

3.2.6. Proposed transport mechanism 54

3.3. Materials and methods 59

3.3.1. Cloning, expression, and purification 59

3.3.2. Selenometihonine-substituted proteins 61

3.3.3. Crystallization of the *E. coli* MetNIQ protein complex and the apo MetQ 62

3.3.4. Heavy-metal derivatives 62

3.3.5. Crystallization of a MetQ homologous protein 62

3.3.6. Data collection and structure determination 63

3.3.7. In vivo transport assays 64

3.3.8. Qualitative determination of complex formation 65

3.3.9. Isothermal titration calorimetry 65

Bibliography 69

Chapter 4: Conclusion 74

LIST OF FIGURES AND TABLES

Figure 1.1. Controversial proposed mechanistic models of the type-I maltose transporter 3

Figure 2.1. Detection of MetNIQ complex formation 18

Figure 2.2. The crystal structure of *E. coli* L-methionine-bound MetQ 20

Figure 2.3. Screening for substrate-binding-deficient MetQ mutants 22

Figure 2.4. Dissociation constants between MetNI and MetQ 24

Table 2.1. Data processing and refinement statistics 31

Figure 3.1. Structure of MetNIQ complex 41

Figure 3.2. Translocation pathways of different ABC importers at a glance 43

Figure 3.3. An unexpected third conformation of MetQ in complex with MetNI 45

Figure 3.4. Potential substrate pathways for the MetNIQ complex 46

Figure 3.5. Conformational changes of the cytoplasmic, periplasmic gates, and C2 domains of the MetNIQ complex 47

Figure 3.6. Hydrogen-bonding shifts at the interface of C2 domains 48

Figure 3.7. The effects of L-methionine to MetNIQ complex formation and stability 50

Table 3.1. Summary of kinetic constants for transport activity of MetNIQ variants 53

Figure 3.8. *In vivo* uptake of MetNIQ and its variants 54

Figure 3.9. Proposed mechanistic atomic model of the methionine transporter 56

Table 3.2. Summary of dissociation constants of methionine to MetNI/MetQ 57

Figure 3.10. Ellipsoidal truncation and anisotropic scaling of strong anisotropic data 58

Figure 3.11. Principal component analysis of the methionine structures 59

Table 3.3. Data collection and refinement statistics for apo MetQ crystal 66

Table 3.4. Data collection and refinement statistics for MetNIQ crystal (after ellipsoidal truncation and anisotropic scaling) 67

Figure 4.1. 2.95 Å resolution crystal structure of the MetNIQ complex 74

Figure 4.2. Structural insights of transport regulation by transinhibition 75

Figure 4.3. Binding of L-methionine substrate by MetQ at atomic resolution 76

Figure 4.4. Thermodynamic sequential binding events of the MetNI methionine transport system 77

Figure 4.5. Proposed mechanistic atomic model of the methionine transporter 79

NOMENCLATURE

ABC	ATP-Binding-Cassette
ADP	Adenosine Diphosphate
AGS	Adenosine γ-phosphate
ATP	Adenosine triphosphate
BN PAGE	Blue-Native Poly-Acryrilamide Gel Electrophoresis
EDTA	(Ethylenedinitrilo)tetraacetic acid
Gu-HCl	Guanidine HCl
ICP-MS	Inductively Coupled Plasma Mass Spectrometry
Met	Methionine
NBD	Nucleotide-binding domain
SBP	Substrate-binding protein
SDS PAGE	Sodium Dodecyl Sulfate
TCEP	Tris(2-carboxyethyl)phosphine hydrochloride
TMD	Transmembrane domain

CHAPTER 1: INTRODUCTION

1.1. Introduction to ABC transporters and the *E. coli* methionine-ABC transporter

ATP-Binding-Cassette (ABC) transporters compose one of the largest protein families and play a variety of physiological roles, including the transport of a diversity of substrates in all species from microbes to humans [1–3]. In microorganisms, ABC transporters are crucial for nutrient uptake, the removal of toxins, and antibiotic resistance [1–3]. In humans, many of the transporters are clinically relevant, such as the cystic fibrosis transmembrane conductance regulator (CFTR) in the development of cystic fibrosis, and the multidrug-resistance transporter, P-glycoprotein (Pgp), in cancer cell survival [1,4,5].

While studies on eukaryotic ABC transporters are still underway, many fundamental principles of ABC transporters have been derived from structural and biochemical characterizations of their bacterial/archaeal homologs. About 5% of the *E. coli* genome has been classified as encoding ABC transporters (Blattner et al., 1997; Linton and Higgins, 1998, Rees, Johnson, & Lewinson, 2009). Our work focuses on the structural characterization of a high-affinity methionine-ABC transport system from *Escherichia coli* K-12. These proteins are highly conserved in bacteria [7], and are important for the infectivity and survival of several human pathogens ([8–11]; note: MetNI is misidentified in the first two references).

1.2. Background

ABC transporters consist of four domains: two transmembrane domains (TMDs) that form the translocation pathway, and two nucleotide-binding domains (NBDs) that use the energy from ATP binding and hydrolysis to fuel transport [1,2,6,12]. ABC importers,

mostly found in prokaryotes, archaea, and plants, require additional domains, such as substrate-binding domains located in the periplasm of Gram-negative bacteria or tethered to the membrane in Gram-positive bacteria and archaea, to bind and deliver substrates to their cognate transporters (Ames et al., 1992; Wilkinson and Verschueren, 2003; Berntsson et al., 2010).

In general, the ABC transporter cycle utilizes a mechanism called the alternating access model [13] that involves the interconversion of two distinct conformations: an inward-facing and outward-facing conformation that opens the translocation pathway to the cytoplasm and periplasm, respectively.

Despite numerous biochemical and structural characterization reports on ABC uptake systems [14–18], only two nutrient uptake systems, the maltose uptake system, $MalFGK_2$, and the vitamin B_{12} uptake system, BtuCD, have been studied extensively [19,20]. These models were built on the structural determinations of different conformations of $MalFGK_2$ and BtuCD transporters during their transport cycles [16,19–22]. Though both transporters share the same overall alternating access model, structures of these transporters in complex with their binding proteins have demonstrated differences in the details of their transport mechanisms. For example, studies by Oldham and colleagues highlight a unique pre-translocation intermediate conformation during the maltose transport cycle, where a liganded maltose-binding protein (MalE) first engages with an inward facing conformation of $MalFGK_2$ [19] (Fig 1.1b). Works by Korkhov and colleagues on the vitamin-B12 transporter identified a two-cytoplasmic-gate system that ensures the substrate specificity [21].

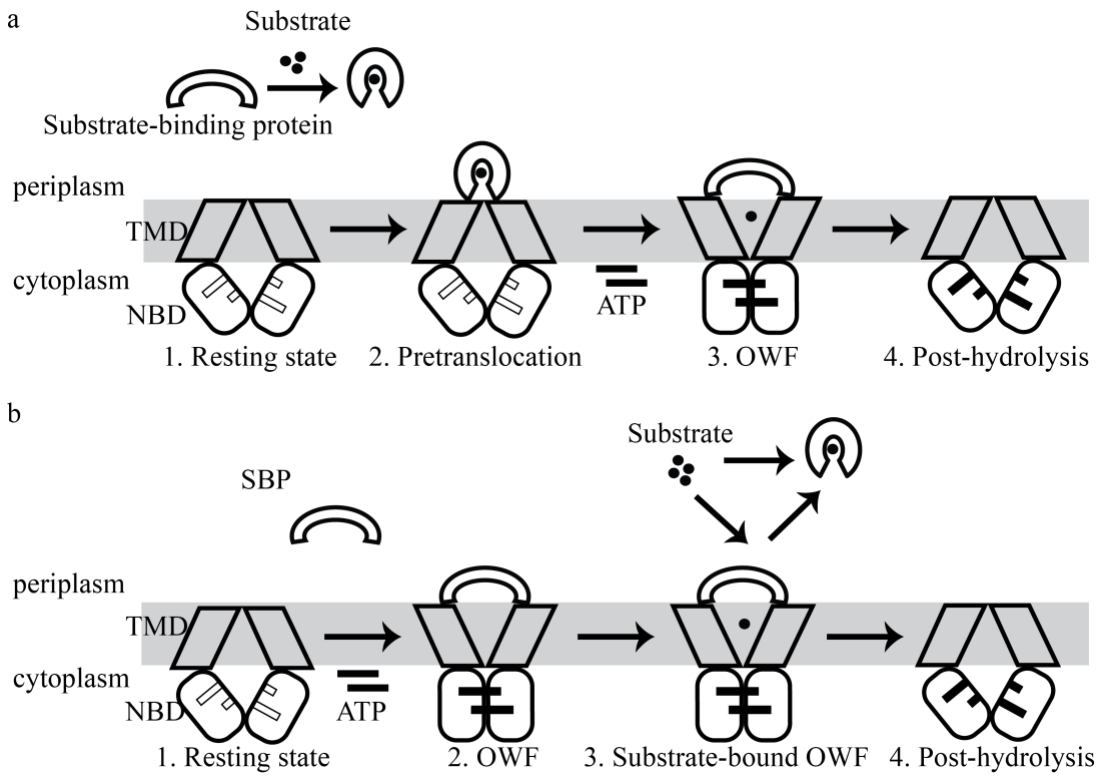

Figure 1.1. Proposed mechanistic models of the Type-I maltose transporter based on structural works (a) from Dr. Jue Chen's group and biochemical works (b) from Dr. Frank Duong's group.

In this work, we focus on the structural characterizations of the *Escherichia coli* high-affinity methionine uptake system (Kadner, 1974), comprising the MetNI transporter and its cognate binding-protein, MetQ (Gál et al., 2002; Merlin et al., 2002). Like a typical ABC transporter, the MetNI transporter consists of four polypeptides: two copies of a trans-membrane subunit (MetI), and two copies of a nucleotide-binding subunit (MetN) [23,24]. Currently, only the inward facing conformation of the *E. coli* methionine-ABC transporter has been determined structurally (Kadaba et al., 2008; Johnson et al., 2012). Crystallographic structures of this transporter notably revealed an additional domain at the

C-terminus of the MetN subunit, termed the C-regulatory or C2 domain [18,24]. This domain is involved in trans-inhibition [25], whereby binding of L-methionine to this domain stabilizes the inactive form of the MetN ATPase domain and the inward-facing conformation of MetNI (Kadaba et al., 2008; Johnson et al., 2012).

1.3. Statement of problems

Controversial proposed mechanistic models for Type-I ABC importers

Equilibrium studies (Bao & Duong, 2013) on the prototypic type-I maltose importer, $MalFGK_2$, contradict the mechanistic models inferred from structural information [16,19]. Nanodisc-based equilibrium studies on the maltose uptake system favor a model in which the outward-facing-conformation of the transporter is triggered by ATP binding alone. This conformation then assembles with unliganded MalE to form a $MalFGK_2$-E complex, to which maltose subsequently binds (Fig 1.1b) (Bao & Duong, 2013) . This observation is different from what X-ray crystallographers have reported for the translocation intermediate state mentioned above, which suggested that the outward-facing conformation is triggered by the binding of liganded MalE to the inward-facing conformation [19].

Transinhibition, a distinct regulation feature, may indicate different mechanistic model for the methionine transporter

Trans-inhibition, best characterized by studies on the *E. coli* MetNI and *Methanosarcina acetivorans* ModBC transporters [18,29,30], has not been observed in either the maltose or vitamin-B_{12} uptake systems. Therefore, current proposed mechanistic

models of the type-I maltose transporter are inadequate to fully explain the methionine uptake system.

Little is known about how the binding protein grasps its substrate and how the transporter and its binding partner engage for substrate delivery

Although structures of individual proteins of the methionine transport system, including the MetNI transporter and the MetQ binding protein, have been solved, little is known about how the binding protein engages and delivers the substrate to the MetNI transporter.

1.4. Primary research questions

Thus far only the inward-facing (IWF) conformation of MetNI has been solved, in a trapped, inhibited state (CY5 form) [18,24]. To build a comprehensive mechanistic model for the MetNIQ transport system, we sought to find answers to the following questions: (1) How does the binding protein interact with its transporter? (2) How do the C-regulatory domains regulate the transport of methionine? (3) How does the binding protein bind or release its substrate? (4) What is the sequential order of interactions among the MetQ binding protein, the MetNI transporter, ATP, and methionine? And finally (5) what is the mechanistic model for the MetNI methionine transporter?

1.5. Significance of study

The structure of the methionine-ABC transporter in complex with its binding protein would address key questions, such as how the transporter and its binding protein work together to acquire methionine for bacteria, and how the transport is regulated by the C-regulatory domains.

A solid mechanistic transport model can be proposed by combining structural findings with biochemical and biophysical characterizations. This model can be applied to the study of other amino acid transporters, Type-I homodimeric ABC importers, and other transport systems ruled by trans-inhibition.

Understanding the regulation of ABC transporters would also aid in the design of better antibiotics and anticancer drugs.

1.6. Research Design

(1) How does the binding protein interact with its transporter?

We sought to determine the structure of the outward-facing conformation MetNI in complex with its binding partner, MetQ. We would first identify conditions under which the MetNI transporter forms a stable complex with the cognate periplasmic binding protein MetQ. We developed a qualitative method to observe the association of the MetNI transporter to MetQ, using gel filtration and BN PAGE. Furthermore, in collaboration with Dr. Qiwen Li, we measured the dissociation constants of MetNI to MetQ using Microscale Thermophorensis techniques. We then crystallized the MetNIQ complex and solved the structure of the complex to reveal the interaction between the MetNI transporter and its MetQ binding protein.

(2) How does the C-regulatory domains regulate transport of methionine?

To elucidate the mechanism that underlies transport regulation, we sought to characterize structural changes of the C-regulatory domains in two conformational states, IWF and OWF conformations, of the MetNI transporter. L-methionine was soaked into crystals of MetNI to see how it stabilizes the IWF conformation of MetNI.

(3) How does the binding protein bind or release its substrate?

To elucidate how the binding protein MetQ binds methionine, we sought to determine the crystal structure of MetQ in its substrate-free form and compare it to the substrate-bound MetQ structure. A co-purifying methionine was observed in the crystal structures of the substrate-binding protein, MetQ [31]. We developed an approach to use alanine-scanning mutagenesis to identify MetQ mutants that disrupt the binding of L-methionine. This mutant would be used as a substrate-free form of MetQ for crystallization purposes.

(4) What is the sequential order of interactions among the MetQ binding protein, the MetNI transporter, ATP, and methionine?

To address the question of the sequential interaction between the binding protein, the transporter, and the substrate, we sought to observe the binding affinities (K_d) of the binding protein to its substrate and to its transporter.

(5) What is the mechanistic model for the MetNI methionine transporter?

To propose a mechanistic model for the MetNI methionine transporter, we biochemically characterized functions of the MetNI methionine transporter by in vivo transport assays. We then combined structural insights with thermodynamic binding constants determined from (4), along with kinetic transport constants, to propose an atomic-level mechanistic model for the MetNI methionine transporter.

1.7. Outline of thesis

In Chapter 2, I present the work on stabilizing the complex of MetNIQ in solution. Preparation of the stable MetNIQ complex in solution was a key for determining its crystal structure mentioned in chapter 3.

In Chapter 3, I present the crystal structure of the MetNIQ complex in a catalytic intermediate state. Combining structural information, enzyme kinetic, and equilibrium studies, I propose a mechanistic model for the methionine transporter.

In Chapter 4, I summarize our results, answer relevant questions raised by the findings, and conclude with a discussion of the results.

BIBLIOGRAPHY

1. Higgins CF. ABC transporters: from microorganisms to man. *Annu Rev Cell Biol*. 1992; 8:67-113. doi:10.1146/annurev.cb.08.110192.000435.

2. Linton KJ, Higgins CF. MicroGenomics The *Escherichia coli* ATP-binding cassette (ABC) proteins. *Mol Microbiol*. 1998; 28:5-13.

3. Higgins CF. ABC transporters: physiology, structure and mechanism--an overview. *Res Microbiol*. 2001; 152(3-4):205-210. http://www.ncbi.nlm.nih.gov/pubmed/11421269.

4. Fletcher JI, Haber M, Henderson MJ, Norris MD. ABC transporters in cancer: more than just drug efflux pumps. *Nat Rev Cancer*. 2010; 10(2):147-156. doi:10.1038/nrc2789.

5. Leonard GD, Fojo T, Bates SE. The role of ABC transporters in clinical practice. *Oncologist*. 2003; 8(5):411-424. doi:10.1634/theoncologist.8-5-411.

6. Rees DC, Johnson E, Lewinson O. ABC transporters: the power to change. *Nat Rev*

Mol Cell Biol. 2009; 10(3):218-227. doi:10.1038/nrm2646.

7. Rodionov D a, Vitreschak AG, Mironov A a, Gelfand MS. Comparative genomics of the methionine metabolism in Gram-positive bacteria: a variety of regulatory systems. *Nucleic Acids Res*. 2004; 32(11):3340-3353. doi:10.1093/nar/gkh659.

8. Chanyangam M, Smith a L, Moseley SL, Kuehn M, Jenny P. Contribution of a 28-kilodalton membrane protein to the virulence of *Haemophilus influenzae*. *Infect Immun*. 1991; 59(2):600-608.

9. Pattery T, Hernalsteens J, Greve H De. Identification and molecular characterization of a novel *Salmonella enteritidis* pathogenicity islet encoding an ABC transporter. 1999; 33(4): 791-805.

10. Shelver D, Rajagopal L, Harris TO, Rubens CE. MtaR , a Regulator of Methionine Transport , Is Critical for Survival of Group B *Streptococcus in vivo*. 2003. doi:10.1128/JB.185.22.6592.

11. Bryan JD, Liles R, Cvek U, Trutschl M, Shelver D. Global transcriptional profiling reveals *Streptococcus agalactiae* genes controlled by the MtaR transcription factor. *BMC Genomics*. 2008; 9:607. doi:10.1186/1471-2164-9-607.

12. Higgins CF, Linton KJ. The ATP switch model for ABC transporters. *Nat Struct Mol Biol*. 2004; 11(10):918-926. doi:10.1038/nsmb836.

13. Jardetzky O. Simple allosteric model for membrane pumps. *Nature*. 1966; 211(5052):969-970. doi:10.1038/211969a0.

14. Hollenstein K, Frei DC, Locher KP. Structure of an ABC transporter in complex with its binding protein. *Nature*. 2007; 446:213-216. doi:10.1038/nature05626.

15. Locher KP, Lee AT, Rees DC. The *E. coli* BtuCD structure: a framework for ABC transporter architecture and mechanism. *Science*. 2002; 296(5570):1091-1098. doi:10.1126/science.1071142.

16. Oldham ML, Khare D, Quiocho FA, Davidson AL, Chen J. Crystal structure of a catalytic intermediate of the maltose transporter. *Nature*. 2007;450:515-522. doi:10.1038/nature06264.

17. Gerber S. Structural Basis of Trans-Inhibition in a Molybdate/Tungstate ABC transporter. *Science (80-)*. 2008;246(2008). doi:10.1126/science.1156213.

18. Kadaba NS, Kaiser JT, Johnson E, Lee A, Rees DC. The high affinity *E. coli* methionine ABC transporter: structure and allosteric regulation. *Science*. 2008;321(5886):250-253. doi:10.1126/science.1157987.

19. Oldham ML, Chen J. Crystal Structure of the Maltose Transporter in a Pretranslocation Intermediate State. *Science*. 2011; 1202-1205. doi:10.1126/science.1200767.

20. Korkhov VM, Mireku S a, Veprintsev DB, Locher KP. Structure of AMP-PNP-bound BtuCD and mechanism of ATP-powered vitamin B12 transport by BtuCD-F. *Nat Struct Mol Biol*. 2014; 21(12):1097-1100. doi:10.1038/nsmb.2918.

21. Korkhov VM, Mireku S a, Locher KP. Structure of AMP-PNP-bound vitamin B12 transporter BtuCD-F. *Nature*. 2012; 490(7420):367-372. doi:10.1038/nature11442.

22. Khare D, Oldham ML, Orelle C, Davidson AL, Chen J. Alternating access in maltose transporter mediated by rigid-body rotations. *Mol Cell*. 2009; 33(4):528-536. doi:10.1016/j.molcel.2009.01.035.

23. Kadaba NS. The high-affinity *E. coli* methionine ABC transporter: structure and allosteric regulation. *Science*. 2008; 321:250-253. doi:10.1126/science.1157987.

24. Johnson E, Nguyen PT, Yeates TO, Rees DC. Inward facing conformations of the MetNI methionine ABC transporter: Implications for the mechanism of transinhibition. *Protein Sci*. 2012; 21(1):84-96. doi:10.1002/pro.765.

25. Kadner RJ. Regulation of methionine transport activity in *Escherichia coli*. *J Bacteriol*. 1975; 122(1):110-119.

26. Lewinson O, Lee AT, Locher KP, Rees DC. A distinct mechanism for the ABC transporter BtuCD – BtuF revealed by the dynamics of complex formation. *Nat Publ Gr*. 2010; 17(3):332-338. doi:10.1038/nsmb.1770.

27. Korkhov VM, Mireku S a, Veprintsev DB, Locher KP. SI_Structure of AMP-PNP-bound BtuCD and mechanism of ATP-powered vitamin B12 transport by BtuCD-F. *Nat Struct Mol Biol*. 2014; (c):2-7. doi:10.1038/nsmb.2918.

28. Bao H, Duong F. ATP alone triggers the outward facing conformation of the maltose ATP-binding cassette transporter. *J Biol Chem*. 2013; 288(5):3439-3448. doi:10.1074/jbc.M112.431932.

29. Yang JG, Rees DC. The Allosteric Regulatory Mechanism of the *Escherichia coli* MetNI Methionine ATP Binding Cassette (ABC) Transporter. *J Biol Chem*. 2015; 290(14):9135-9140. doi:10.1074/jbc.M114.603365.

30. Gerber S, Comellas-Bigler M, Goetz B a, Locher KP. Structural basis of trans-inhibition in a molybdate/tungstate ABC transporter. *Science*. 2008; 321(5886):246-250. doi:10.1126/science.1156213.

31. Kadaba NS. Structure studies of the *Escherichia coli* methionine ABC transporter and its cognate binding protein. 2008.

32. Locher KP. Mechanistic diversity in ATP-binding cassette (ABC) transporters. *Nat Struct Mol Biol*. 2016; 23(6):487-493. doi:10.1038/nsmb.3216.

33. Widdas WF. Inability of diffusion to account for placental glucose transfer in the sheep and consideration of the kinetics of a possible carrier transfer. *J Physiol*. 1951; (118):23-39.

34. Hollenstein K, Dawson RJP, Locher KP. Structure and mechanism of ABC transporter proteins. *Curr Opin Struct Biol*. 2007; 17(4):412-418. doi:10.1016/j.sbi.2007.07.003.

35. Hvorup RN, Goetz B a, Niederer M, Hollenstein K, Perozo E, Locher KP. Asymmetry in the structure of the ABC transporter-binding protein complex BtuCD-BtuF. 2007; 317:1387-1390. doi:10.1126/science.1145950.

36. Oldham ML, Chen S, Chen J. Structural basis for substrate specificity in the *Escherichia coli* maltose transport system. *Proc Natl Acad Sci U S A*. 2013; 110(45):18132-18137. doi:10.1073/pnas.1311407110.

37. Bao H, Duong F. Discovery of an auto-regulation mechanism for the maltose ABC transporter MalFGK2. *PLoS One*. 2012; 7(4):e34836. doi:10.1371/journal.pone.0034836.

38. Goudsmits JMH, Jan Slotboom D, van Oijen AM. Single-molecule visualization of conformational changes and substrate transport in the vitamin B12 ABC importer BtuCD-F. *Nat Commun*. 2017;8(1):1652. doi:10.1038/s41467-017-01815-7.

39. Nguyen PT, Li QW, Kadaba NS, Lai JY, Yang JG, Rees DC. The contribution of methionine to the stability of the *Escherichia coli* MetNIQ ABC transporter-substrate binding protein complex. *Biol Chem*. 2015; 396(9-10):1127-1134. doi:10.1515/hsz-2015-0131.

40. Kadner RJ, Watson WJ. Methionine Transport in *Escherichia coli*: Physiological and Genetic Evidence for Two Uptake Systems. *J Bacteriol*. 1974; 119(2):401-409.

41. Zhang Z, Feige JN, Chang AB, et al. A transporter of *Escherichia coli* specific for L- and D-methionine is the prototype for a new family within the ABC superfamily. *Arch Microbiol*. 2003; 180(2):88-100. doi:10.1007/s00203-003-0561-4.

42. Kadner RJ. Transport and utilization of D-methionine and other methionine sources in *Escherichia coli*. *J Bacteriol*. 1977; 129(1):207-216.

43. Studier FW. Protein production by auto-induction in high density shaking cultures. *Protein Expr Purif*. 2005; 41(1):207-234. doi:10.1016/j.pep.2005.01.016.

44. Strong M, Sawaya MR, Wang S, Phillips M, Cascio D, Eisenberg D. Toward the structural genomics of complexes: Crystal structure of a PE/PPE protein complex from Mycobacterium tuberculosis. *Proc Natl Acad Sci*. 2006; 103(21):8060-8065. doi:10.1073/pnas.0602606103.

45. Adams PD, Grosse-Kunstleve RW, Hung LW, et al. PHENIX: Building new software for automated crystallographic structure determination. *Acta Crystallogr Sect D Biol Crystallogr*. 2002; 58(11):1948-1954. doi:10.1107/S0907444902016657.

46. Dimaio F, Echols N, Headd JJ, Terwilliger TC, Adams PD, Baker D. Improved low-

resolution crystallographic refinement with Phenix and Rosetta. *Nat Methods*. 2013; 10(11):1102-1106. doi:10.1038/nmeth.2648.

47. Collaborative Computational Project N 4. The CCP4 suite: programs for protein crystallography. *Acta Crystallogr D Biol Crystallogr*. 1994; 50(5):760-763. doi:10.1107/S0907444994003112.

48. Emsley P, Cowtan K. Coot: Model-building tools for molecular graphics. *Acta Crystallogr Sect D Biol Crystallogr*. 2004; 60(12 I):2126-2132. doi:10.1107/S0907444904019158.

49. Gouridis G, Schuurman-wolters GK, Ploetz E, et al. Conformational dynamics in substrate-binding domains influences transport in the ABC importer GlnPQ. 2015;22(1). doi:10.1038/nsmb.2929.

CHAPTER 2

THE CONTRIBUTION OF METHIONINE TO THE STABILITY OF THE *ESCHERICHIA COLI* METNIQ ABC TRANSPORTER - SUBSTRATE BINDING PROTEIN COMPLEX

Published as Nguyen, P.T, Li, Q.W., Kadaba, N.S., Lai, J.Y., Yang J.G., Rees, D.C. "The contribution of methionine to the stability of the *Escherichia coli* MetNIQ ABC transporter-substrate binding protein complex." Biol Chem. 396(9–10), 1127–34. (2015)

2.1. Introduction

Many different transporters are encoded in the genomes of microorganisms to accommodate the diversity of molecules they need to acquire from the environment. For example, ~10% of the *E. coli* genome has been classified as participants in transport processes, of which approximately half are ATP-binding cassette (ABC) transporters [1,2]. ABC transporters consist of four domains: two transmembrane domains (TMDs) that form the translocation pathway, and two nucleotide-binding domains (NBDs) that use the energy from ATP binding and hydrolysis to fuel transport (reviewed in (Ames et al., 1992; Higgins, 1992; Holland et al., 2003; Locher, 2008; Oldham et al., 2008; Rees et al., 2009)). The transport mechanism utilizes an alternating access model (Widdas, 1952; Jardetsky, 1966) that involves the interconversion of two distinct conformations during the transport cycle, inward facing and outward facing, where the translocation pathway is open to the cytoplasm and periplasm, respectively. ABC importers, mostly found in prokaryotes, archaea and plants, require an additional component for transport, namely substrate-binding proteins (SBP), located in the periplasm of Gram-negative bacteria or tethered to the membrane in Gram-positive bacteria and archaea, to bind and deliver substrates to their

cognate transporter (Ames et al., 1992; Wilkinson and Verschueren, 2003; Berntsson et al., 2010). Structures of transporters in complex with their binding proteins (Hollenstein et al., 2007; Hvorup et al., 2007; Oldham et al., 2007; Korkhov et al., 2012) have been instrumental in defining basic features of the transport cycle, including the two best structurally characterized ABC importers, the Type I maltose uptake system, $MalFGK_2$ (Oldham and Chen, 2011) and the Type II vitamin B_{12} uptake system, BtuCD (Korkhov et al., 2014). Despite the common nucleotide-dependent engine driving translocation, binding protein - transporter interactions can vary significantly, reflecting mechanistic diversity between various ABC importers (Lewinson et al., 2010).

In this work, we focus on the *Escherichia coli* high affinity methionine uptake system (Kadner, 1974), comprising the MetNI transporter and its cognate binding-protein, MetQ (Gál et al., 2002; Merlin et al., 2002). Currently, only the inward facing conformational state of MetNI has been solved crystallographically (Kadaba et al., 2008; Johnson et al., 2012). To build a comprehensive model for MetNI transport, we sought to identify conditions under which a stable transporter-binding protein complex can form. A challenge in working with *E. coli* MetNI is that while methionine is the transported ligand, it also functions as an allosteric effector inhibiting methionine uptake at sufficiently high intracellular concentrations (Kadner, 1975). This phenomenon of transinhibition is mediated by methionine functioning as a noncompetitive inhibitor of ATPase activity (Yang and Rees, 2015) by binding to a cytoplasmic regulatory domain of the ABC subunit MetN to stabilize MetNI in an inward facing conformation incapable of hydrolyzing ATP (Kadaba et al., 2008; Johnson et al., 2012). Further complicating the analysis is the observation of a co-purifying methionine in crystal structures of methionine binding SBPs

(Deka et al., 2004; Williams et al., 2004; Yang et al., 2009; Yu et al., 2011), including the *E. coli* MetQ structure (Kadaba, 2008).

Here we demonstrate that formation of a high affinity MetNIQ complex requires an ATP-bound state of MetNI and an unliganded form of MetQ. Preparation of this complex is facilitated by the identification of mutations in MetQ that abolish methionine binding. The effect of methionine on complex formation between ATP-stabilized MetNI and MetQ is quantitated by titrating fluorescently labeled MetQ with varying concentrations of MetNI. From these measurements, dissociation constants of 1100 ± 300 and 27 ± 9 nM are found for methionine-bound and methionine free MetQ, respectively, establishing that ligand-free MetQ can form a stable complex with the ATP-bound form of MetNI. Our isolation of a stable MetNIQ complex is an essential step towards the crystallographic analysis of the outward facing conformation, a key intermediate in the uptake of methionine by this transporter.

2.2. Results and discussion

To better understand the mechanism of the methionine transport system, we sought to identify conditions under which the MetNI transporter forms a stable complex with the cognate periplasmic binding protein MetQ. Previous studies demonstrated that wild type MetNI and wild type MetQ interact weakly in the absence of nucleotide (K_d = 7.4 x 10^{-5} M) and a stable complex under these conditions could not be detected by gel filtration chromatography (Lewinson et al., 2010). Based on studies of the maltose system (Chen et al., 2001), we hypothesized that the MetNI transporter binds MetQ with the highest affinity in an ATP-bound state. To maintain the ATP-bound state, an ATPase deficient form was generated by substitution of Glu 166 in the Walker B motif of MetN with Gln (E166Q), in

combination with the use of the chelator EDTA with ATP to remove the catalytically essential Mg^{2+}. Mutation of the Walker B Glu is commonly used to inhibit hydrolysis, but not binding, of ATP by ABC transporters (Moody et al., 2002)

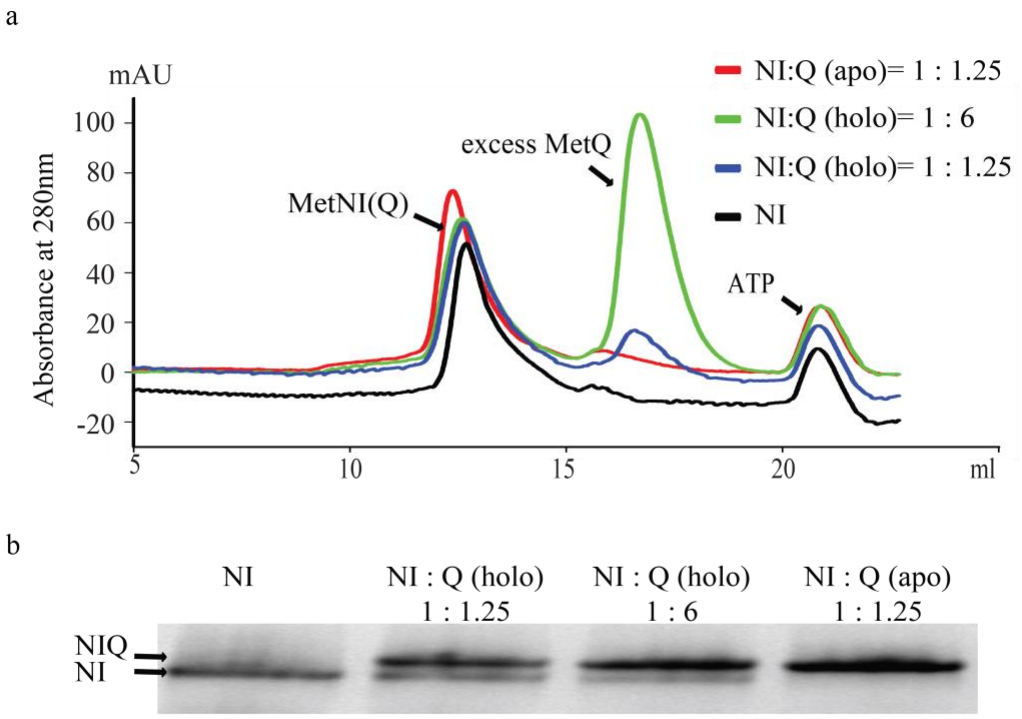

Figure 2.1. Detection of MetNIQ complex formation

a. Gel filtration for detection of complex formation. Reactions of E166Q MetNI (40 µM) and MetQ at the indicated molar ratios in the presence of 1 mM ATP and 1 mM EDTA were injected onto a size exclusion column. The highest A_{280} eluate peak was analyzed by BN PAGE.

b. BN PAGE of the highest peak from the schematic shown in A. Lane 1: E166Q MetNI alone, lanes 2 and 3: wild type MetQ added to E166Q MetNI at different ratios, 1:1.25 and

1:6 (MetNI: MetQ), lane 4: N229A MetQ added to E166Q MetNI at 1:1.25 (MetNI: MetQ) ratio.

ATPase assays show that the E166Q mutation results in a 20-fold reduction in ATPase activity (data not shown). All subsequent experiments in this study were conducted using this mutant transporter, denoted E166Q MetNI, in the presence of saturating amounts of ATP+EDTA (1 mM ATP and 1 mM EDTA) to mimic the ATP-bound state.

We first tested for complex formation by incubating E166Q MetNI with wild type MetQ and saturating amounts of ATP+EDTA at different ratios of transporter to binding protein. Mixtures of either 1:1.25 or 1:6 (MetNI: MetQ) were injected onto a gel filtration column (Fig 2.1a), and the peak fraction was analyzed by blue native PAGE (BN PAGE (Reisinger and Eichacker, 2006)) (Fig 2.1b) to evaluate the extent of complex formation. Despite an excess of MetQ, incomplete complex formation was observed in both cases (Fig 2.1b., lanes 2 and 3), as established by the presence of two bands on BN PAGE, the upper one corresponding to the MetNIQ complex and the lower one to free transporter by comparison to E166Q MetNI alone (Fig 2.1b., lane 1).

Wild type MetQ contains a co-purifying methionine identified in the crystal structures of MetQ homologs S. aureus lipoprotein-9 (PDB entry 1P99, (Williams et al., 2004)), *T. pallidium* Tp32 (PDB entry 1XS5, (Deka et al., 2004)), *E. coli* MetQ (Kadaba, 2008), *N. meningitides* (PDB 3IR1, (Yang et al., 2009)), *V. vulnificus* (PDB 3K2D, (Yu et al., 2011)) and unpublished structures with PDB entries 3TQW, 3UP9, 4EF1, 4GOT, 4IB2, 4K3F, 4QHQ, 4QYM, and 4Q5T. The basic structure and binding site for L-methionine are illustrated in Fig. 2.2a for *E. coli* MetQ refined at 1.6 Å resolution (PDB entry 4YAH, see Methods). An extensive hydrogen bond/salt bridge network between protein side

chains and the methionine amino and carboxyl groups likely contributes to the tight binding of ligand to MetQ (Fig 2.2b). Groups interacting with the carboxyl group of methionine include the side chains of Arg144, Asn202, and a buried water, while the amino group interacts with the side chains of Glu42 and Thr204 and two buried waters (Fig 2.2b). Significantly, the side chain of Asn229 forms two hydrogen bonds (one each) to the amino and carboxyl groups of the L-methionine (Fig 2.2b). The side chain of the bound L-methionine fits in a pocket surrounded by the aromatic side chains of Tyr69, Phe86, His88, and Tyr91 (Fig 2.2b). Aromatic interactions with the methionine side chain are not uncommon (Pal and Chakrabarti, 2001), particularly the interaction observed with the ligand SD packed against the plane of His88 such that the CG-SD bond is oriented towards the NE2 atom of His88.

a

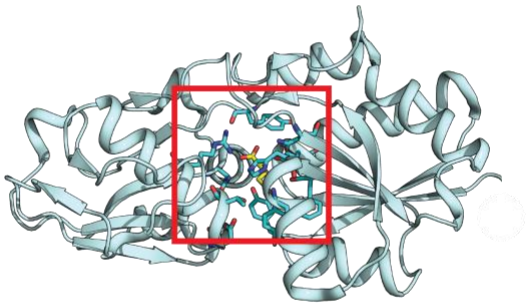

b

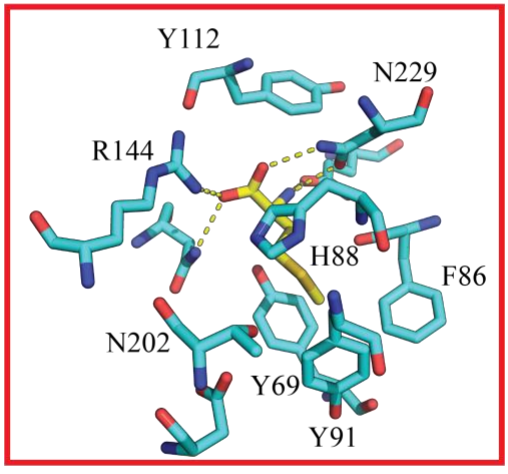

Figure 2.2. The crystal structure of E. coli L-methionine-bound MetQ

a. Ribbon diagram of L-methionine-bound E. coli MetQ.

b. The L-methionine binding site in MetQ. The side chains of the interacting residues are colored green, and the L-methionine substrate is colored grey. Hydrogen bonds between the amino and carboxyl groups of L-methionine and surrounding MetQ residues are represented by yellow dashes.

To evaluate the contribution of L-methionine binding to MetQ to the stability of the MetNIQ complex, it is necessary to prepare ligand-free MetQ. While methionine can be removed from MetQ by an unfolding/refolding process (Deka et al., 2004), we developed an alternative approach of using alanine-scanning mutagenesis to identify MetQ mutants that disrupt the binding of L-methionine. Residues in the MetQ binding pocket in contact with methionine were mutated to alanine (Fig. 2.3), with the exception of Glu42, which was substituted with Gln (E42Q) since the E42A mutant aggregated.

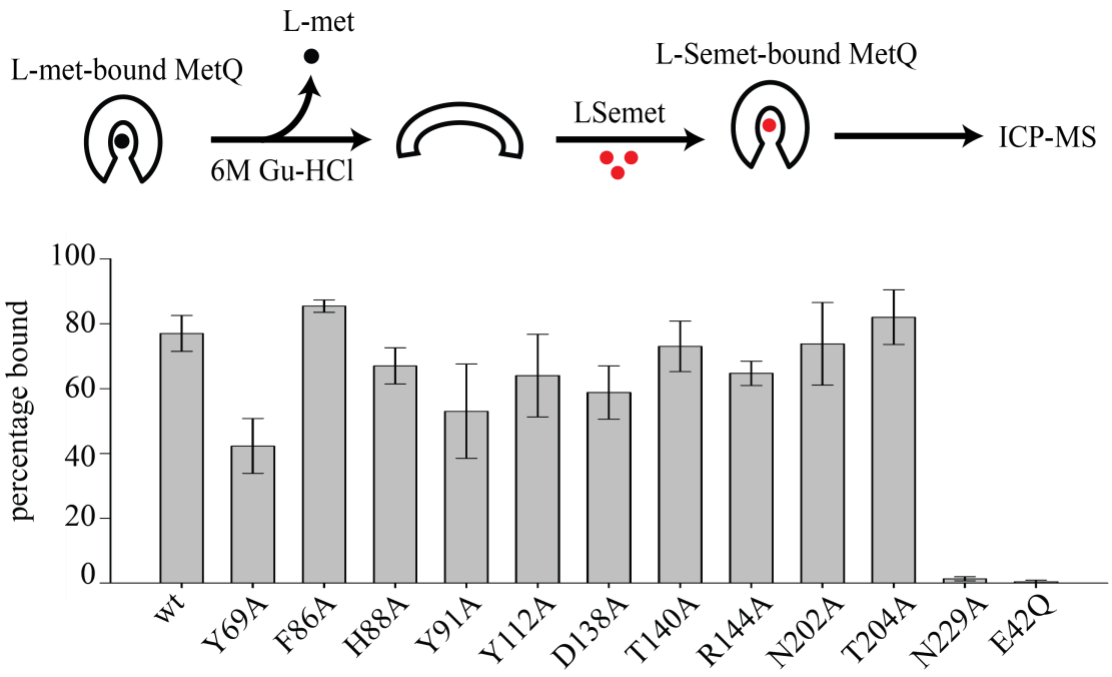

Figure 2.3. Screening for substrate-binding-deficient MetQ mutants

Alanine-scanning mutants of MetQ were analyzed for selenium content by ICP-MS after exchange of native substrate with L-selenomethionine (see text). The horizontal and vertical axes denote the MetQ mutations and fraction of MetQ bound by selenomethionine, respectively. Error bars represent the standard deviation of duplicate samples.

To test for L-methionine binding, we unfolded MetQ in 6 M guanidine-HCl to release any co-purified L-methionine (Deka et al., 2004), and then refolded the protein in the presence of L-selenomethionine. Selenium content was measured by inductively coupled plasma mass spectrometry (ICP-MS), and the molar ratio of selenium to MetQ was calculated (Fig. 2.3). Mutation of Glu42 to Gln (E42Q) and Asn229 to Ala (N229A) significantly decreased the binding affinity of MetQ to selenomethionine, while substitutions at other residues had relatively little effect on selenomethionine binding. The E42Q and N229A MetQ mutants, identified in this screen as unable to bind

selenomethionine (and presumably methionine), were then tested for complex formation with E166Q MetNI in the presence of ATP+EDTA. The E42Q mutant was unable to form a complex with its cognate transporter (data not shown). When N229A MetQ was incubated with E166Q MetNI in the presence of ATP+EDTA, however, stoichiometric complex formation was observed (Fig. 2.1b, lane 4). This result contrasts with the mixture of free and complexed species observed when E166Q MetNI is incubated with wild type liganded MetQ under comparable conditions (Fig. 2.1b, lanes 2 and 3). Based on these results, the N229A MetQ variant was used in this study to mimic methionine-free MetQ.

To quantify the binding affinity of E166Q MetNI for MetQ in either the bound or unliganded state, we measured the dissociation constants for complex formation from titration curves conducted with fluorescently labeled MetQ on a Monolith NT.115 Microscale Thermophoresis Instrument (NanoTemper Technologies GmbH). Wild type and N229A MetQ were labeled with Cy3-maleimide and titrated with varying concentrations of E166Q MetNI in the presence of ATP+EDTA. The fraction of MetQ in complex with E166Q MetNI was calculated from fluorescent intensity values (see Methods). The affinity of L-methionine-bound wild type MetQ for E166Q MetNI was ~40-fold weaker than that for unliganded N229A MetQ to E166Q MetNI (Fig 2.4). The calculated K_d of 1100 ± 300 nM for wild type MetQ represents a lower limit for the affinity, as saturating amounts of E166Q MetNI were prone to aggregation. The K_d for N229A MetQ was determined to be 27 ± 9 nM. This difference in affinity is qualitatively consistent with our BN PAGE results (Fig 2.1b).

We have identified conditions promoting stable complex formation between MetNI and MetQ through the use of two mutations (the E166Q variant in the Walker B motif of

MetN that reduces ATP hydrolysis, and the N229A variant of MetQ that disrupts methionine binding) and the presence of ATP+EDTA to reduce the concentration of Mg^{2+} critical for ATP hydrolysis. These conditions should stabilize the ATP-bound form of MetNI, corresponding to the outward facing conformation of a Type I ABC transporter (Oldham and Chen, 2011). An unexpected feature of the MetNI system is that the use of ligand free MetQ resulted in stable complex formation, in contrast to the maltose transporter system where formation of a stable transporter-SBP complex required the presence of the transported substrate (Chen et al., 2001; Oldham et al., 2007). In the absence of ATP, a "pre-translocation" species has also been crystallized with substrate-loaded SBP and an inward facing conformation of the transporter for the molybdate (Hollenstein et al., 2007) and maltose (Oldham and Chen, 2011) transporters. While the corresponding complex between liganded SBP and the methionine transporter is substantially less stable (K_d ~ 7.5 x 10^{-5} M (Lewinson et al., 2010)) than the complex in the presence of ATP measured in this work (K_d ~ 10^{-6} M), at the protein concentrations (~10^{-4} M) used in crystallization trials, perhaps this state of the MetNIQ complex could also be crystallized under appropriate conditions.

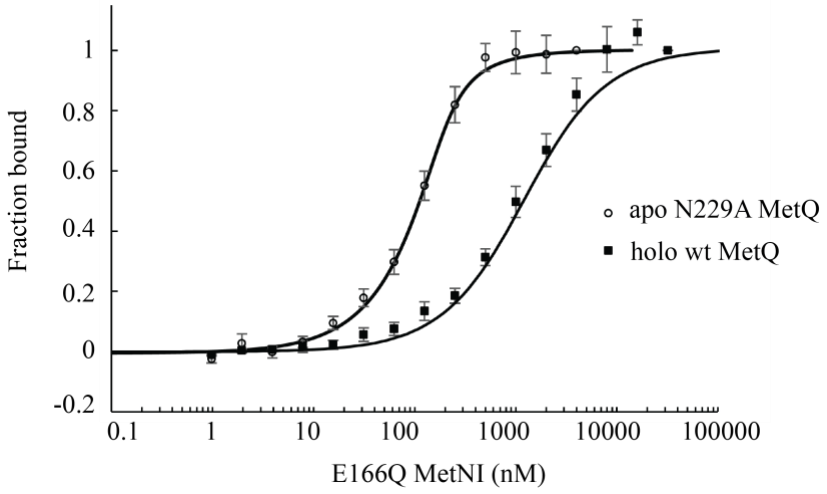

Figure 2.4. Dissociation constants between MetNI and MetQ

The affinity of MetNI for MetQ was measured by titration curves using fluorescently labeled MetQ in the presence or absence of bound methionine (wild type or N229A MetQ, respectively). All experiments contained 1 mM ATP and 1 mM EDTA. 101 nM of Cy3-labeled wild type MetQ was titrated with 1.95 nM – 32 μM non-labeled E166Q MetNI (closed squares). 99 nM of Cy3-labeled N229A MetQ was titrated with 1.95 nM – 4 μM non-labeled MetNI E166Q (open circles). The dissociation constants calculated from these data for wild type (methionine-bound) and N229A (methionine-free) MetQ binding to E166Q MetNI are K_d = 1100 ± 300 nM and 27 ± 9 nM, respectively. Error bars represent standard error from three independent measurements.

The role of transported ligand in complex formation is of great mechanistic interest. For complex formation between MetNI and MetQ, the difference in dissociation constants between unliganded (27 nM) and liganded (1100 nM) MetQ implies that the binding of methionine to MetQ in complex with MetNI is ~40-fold weaker than the binding of methionine to MetQ alone. Energetically, this observation is consistent with a model where the SBP must release ligand for transport to occur. The detailed energetics will certainly depend on the transporter and assay conditions; for example, while liganded maltose binding protein has been reported to more efficiently stimulate ATP hydrolysis of maltose transporter reconstituted into proteoliposomes (Davidson et al., 1992), ligand-free maltose binding protein binds 5-fold more tightly than liganded binding protein to maltose transporter in nanodiscs with AMPPNP (K_d ~ 80 nM and ~400 nM in the absence or presence of maltose, respectively (Bao and Duong, 2012)). An additional complication with the MetNI transporter is that methionine is both a transported ligand and an allosteric

inhibitor of transport, and these effects will need to be distinguished from the contributions of the liganded state of MetQ to the observed kinetics. The development of a detailed molecular transport mechanism will require analysis of conformational dynamics of the type recently described for the GlnPQ uptake system (Gouridis et al., 2015). The structural analysis of stable forms of ABC transporters such as the MetNIQ complex detailed here will provide crucial reference states for these future mechanistic studies.

2.3. Materials and methods

2.3.1. Cloning, expression and purification of MetQ

The metNIQ operon was amplified from *Escherichia coli* K-12 genomic DNA and cloned into a zero blunt pCR-4 TOPO vector as described in (Kadaba et al., 2008). The metQ gene, lacking the stop codon, was subcloned using oligonucleotides that included NdeI and XhoI restriction-enzyme sites, and then ligated into the pET21b(+) vector with a C-terminal 6x-histidine tag. The cloned plasmids were expressed separately in *E. coli* BL21 (DE3) gold cells (EMD) at 37 ℃ in Terrific Broth medium with 100 μg/ml ampicillin. The cells were induced at OD_{600} ~4.0 with 0.4 mM IPTG for 2 hours, then harvested and stored at -80 ℃.

For purification of mature MetQ, periplasmic extract was prepared by resuspending 10 g of cell paste in 10 ml of 40% sucrose, 10 mM Tris-HCl pH 7.5, and 1 mM EDTA, and stirred for one hour at room temperature. The cells were then shocked by addition of 500 ml of ice-cold water. After stirring for 10 min, buffer components were added to a final concentration of 25 mM Tris pH 7.5, 150 mM NaCl, and 17 mM imidazole. The resulting suspension was then centrifuged at 37,500 x g for 30 min to remove all cellular debris from the periplasmic extract. MetQ was isolated from the periplasmic extract by immobilized

metal ion affinity chromatography using a 5 ml Ni-NTA column (GE). The affinity column was washed with 25 mM Tris pH 7.5, 150 mM NaCl, and 17 mM imidazole for 10 column volumes. Protein was then eluted from the column using 25 mM Tris pH 7.5, 100 mM NaCl, and 150 mM imidazole. Peak fractions were dialyzed against 25 mM Tris pH 7.5 and 150 mM NaCl overnight, and then concentrated to 30 mg/ml using a 10kD MWCO concentrator (Millipore).

The full-length protein cloned for this work, including the signal sequence and the C-terminal 6x-his tag, has the sequence:

1 **MAFKFKTFAAVGALIG**SLALVGCGQDEKDPNHIKVGVIVGAEQQVAEVAQKVAKDKYGLD

61 VELVTFNDYVLPNEALSKGDIDANAFQHKPYLDQQLKDRGYKLVAVGNTFVYPIAGYSKK

121 IKSLDELQDGSQVAVPNDPTNLGRSLLLLQKVGLIKLKDGVGLLPTVLDVVENPKNLKIV

181 ELEAPQLPRSLDDAQIALAVINTTYASQIGLTPAKDGIFVEDKESPYVNLIVTREDNKDA

241 ENVKKFVQAYQSDEVYEAANKVFNGGAVKGWLEHHHHHH

The cleaved signal sequence is highlighted in bold, so that the purified protein used in this study consists of residues 17 to 279, of which residues 29-273 (underlined) are observed in the electron density.

2.3.2. Purification of MetNI

Purification of wild type and mutant E166Q MetNI was carried out as described (Johnson et al., 2012) with the one modification that buffer containing 20 mM TAPS pH 8.5, 100 mM NaCl and 0.025% DDM (with varying amounts of imidazole) was used in all purification steps (the original protocol used 250 mM NaCl and different detergents).

2.3.3. MetQ crystallization and structure determination

Crystallization conditions for MetQ were screened with varying concentrations of protein from 15 mg/ml to 60 mg/ml. Crystals were obtained using a hanging drop vapor diffusion method at 20° C, by mixing 1 µl of protein to 1 µl of the following well solution: 24% PEG 4000, 4% PEG 400, 0.1 M sodium citrate pH 5.6, and 0.2 M ammonium acetate at 30 mg/ml of protein, similar to the conditions originally described (Kadaba, 2008). Initial thin needle crystals appeared within a week but crystals were not large enough for data collection. Both microseeding and macroseeding were used to obtain larger crystals, reaching a final size 0.5 x 0.2 x 0.1 mm^3 in a week. The best crystal was obtained by macroseeding with a precipitant 20% PEG 4000, 3% PEG 400, 0.1 M sodium citrate pH 5.6, and 0.2 M ammonium acetate. Diffraction data to 1.6 Å resolution were collected at the Stanford Synchrotron Radiation Lightsource (SSRL) on beamline 12-2. The data was processed using xia2 (Winter, 2010) using XDS (Kabsch, 2010), XSCALE, and AIMLESS (Evans, 2006), with data collection and processing statistics listed in Table 1. Molecular replacement was performed using Phenix (Adams et al., 2010) from the previously solved 1.8 Å resolution MetQ structure (Kadaba, 2008) that was in turn solved by molecular replacement from PDB entry 1P99 (Williams et al., 2004), a Gly-Met-binding protein. The structure was refined with Phenix to 1.6 Å resolution to a final R/Rfree of 0.154/0.183. Coordinates and structure factors have been deposited in the Protein Data Bank of the Research Collaboratory for Structural Bioinformatics, with ID 4YAH.

2.3.4. Screening of substrate-binding deficient MetQ mutants

Individual residues located in the substrate-binding pocket of MetQ were substituted with alanine by site-directed mutagenesis using the Quickchange Mutagenesis kit (Stratagene), with the exception of Glu42, which was substituted with glutamine to

avoid aggregation. To evaluate the binding ability of each mutant for substrate, L-methionine was exchanged with L-selenomethionine, and the amount of selenium was measured using inductively coupled plasma mass spectrometry (ICP-MS).

To exchange L-methionine with L-selenomethionine, individual MetQ mutants immobilized onto Ni-NTA columns were unfolded by washing with 12 column volumes of denaturing buffer containing 6 M guanidine-HCl, 25 mM Tris pH 7.5, 150 mM NaCl at the rate of 1.5 ml/min to remove bound L-methionine. To refold MetQ, guanidine-HCl was slowly removed by flowing renaturation buffer (2 mM L-selenomethionine, 25 mM Tris pH 7.5, 150 mM NaCl) over the column at 1 ml/min for 90 min. The column was further washed with 10 column volumes of renaturation buffer to ensure reloading of MetQ with L-selenomethionine. This was followed by 12 column volumes of wash buffer (25 mM Tris pH 7.5 and 150 mM NaCl) to remove unbound L-selenomethionine. Finally, MetQ was eluted in 25 mM Tris pH 7.5, 150 mM NaCl, and 150 mM imidazole, and run over a size-exclusion column (Superdex 200 16/60, GE Healthcare) equilibrated in 25 mM Tris, pH 7.5 and 150 mM NaCl. The monodisperse peak was collected and concentrated to 20 mg/ml using an Amicon 10-kD MWCO concentrator (Millipore).

The amount of bound L-selenomethionine was measured by quantitation of the selenium content of acid-digested protein samples using ICP-MS. A final concentration of 0.1 μM of protein was digested with 2% trace metal grade nitric acid (Fluka) at 70 ˚C overnight. Samples were centrifuged at 30,000 x g for 10 min using a bench top centrifuge to remove particulate matter. The supernatant was then diluted to a final volume of 5 ml in double distilled H_2O and measured for Se^{78} with an HP 4500 ICP-MS instrument. L-selenomethionine powder stock (Anatrace) was used to prepare standards. Each sample

was measured in duplicate in two independent experiments. Error bars represent standard deviation. Data were processed and graphed using Microsoft Excel and Sigmaplot 11.0, respectively.

2.3.5. Qualitative determination of complex formation

MetNI and MetQ concentrations were measured using a Nanodrop 2000 Spectrophotometer (Thermo Scientific), according to their calculated extinction coefficients for a 1 mg ml^{-1} solution at 280 nm of 0.64 and 0.73, respectively. Complex formation was assessed by mixing E166Q MetNI transporter and its cognate binding protein, MetQ, at a molar ratio of 1:1.25 (MetNI: MetQ) in the presence of 1 mM ATP and 1 mM EDTA. The mixture, containing 40 μM MetNI, 50 μM MetQ, 1 mM ATP, 1 mM EDTA, 20 mM TAPS pH 8.5, 100 mM NaCl, 0.025% DDM, and 5 mM □-mercaptoethanol, was incubated for 1 hour at room temperature and ultracentrifuged at 200,000 x g for 20 min to remove any aggregation. Samples were injected onto a Superdex S200 10/300 sizing column (GE Healthcare) equilibrated with buffer containing 20 mM TAPS pH 8.5, 100 mM NaCl, 0.5 mM ATP, 1 mM EDTA, 0.3% Cymal-5, and 5 mM β-mercaptoethanol. The absorbance reading at 280 nm and the retention volume of the peak were used to follow complex formation. MetNIQ complex formation was verified by analyzing the highest peak by BN PAGE (Reisinger and Eichacker, 2006) using 4-20% Criterion gels (Bio-Rad). Two independent experiments were conducted per condition.

2.3.6. Measurement of MetNIQ complex dissociation constant

The *E. coli* MetQ sequence contains one cysteine residue at amino acid position 23. Purified wild type MetQ and N229A MetQ were labeled with Cy3-maleimide (GE Healthcare), according to the manufacturer's instructions, in buffer containing 25 mM Tris

pH 7.5, 150 mM NaCl, and 10 mM TCEP pH 7.5. Unreacted dye was removed using a Superdex 200 10/300 GL column (GE Healthcare) equilibrated with the aforementioned buffer condition. The label to protein ratio was determined using a NanoDrop 2000 Spectrophotometer (Thermo Scientific) at 550 and 280 nm, and a labeling efficiency of 10% was calculated. Fluorescence measurements were performed on a Monolith NT.115 Instrument (NanoTemper Technologies GmbH) at 25 °C using standard capillaries. Varying concentrations (ranging from 1.95 nM to 32 µM) of unlabeled E166Q MetNI in ATP buffer (1 mM ATP, 1 mM EDTA, 20 mM TAPS pH 8.5, 100 mM NaCl, and 0.3 % Cymal-5) were titrated against a constant concentration of MetQ (101 nM of wild type MetQ or 99 nM of N229A MetQ). Fluorescent intensity as a function of E166Q MetNI concentration was normalized to fraction bound by averaging the intensity values for the lowest three concentrations of E166Q MetNI per experiment. This background intensity was subtracted from all concentrations to yield corrected intensity values. The corrected intensity values were then divided by the corrected intensity at the highest concentration of E166Q MetNI to normalize intensity values to fraction bound values. Dissociation constants for wild type MetQ or N229A MetQ binding to E166Q MetNI were calculated using the K_d Fit function of the NanoTemper Analysis 1.5.41 software. Three independent MST measurements per condition were conducted, and error bars represent standard error of the mean.

Table 2.1. Data processing and refinement statistics

Data Processing Statistics	**MetQ**
Space group	$C222_1$
Unit cell dimensions (a, b, c) (Å)	59.7, 87.4, 112.9

Wavelength (Å)	1.00
Resolution (Å)[a]	24.5-1.60 (1.64 – 1.60)
Unique reflections	38,555
Redundancy	4.1
Completeness (%)	98.4 (96.1)
I / σ	11.5(1.11)
R_{merge}	0.07 (0.952)
Refinement Statistics	**PDB ID 4YAH**
Resolution (Å)[a]	24.5 – 1.60 (1.64 – 1.60)
R-work	0.154 (0.360)
R-free	0.183 (0.409)
Average B factor (Å)	27.7
RMSD bond length (Å)	0.008
RMSD bond angle (°)	1.21
Ramachandran plot (favored, allowed, outliers, %)	98, 2, 0

[a]Numbers in parentheses represent data in the highest resolution shell

Acknowledgments

A Vietnam International Education Development scholarship from the Vietnam Ministry of Education and Training scholarship to P.T.N, an NSF Graduate Fellowship to Q.W.L., and support of NIH Predoctoral Training Grant T32 GM07737 to N.S.K., are gratefully acknowledged. We thank Allen Lee for generating the original MetNIQ constructs, Christoph Müller for MetNIQ discussions, and Dr. Jens Kaiser and Dr. Nathan Dalleska for assistance with crystallography and ICP-MS, respectively. We gratefully acknowledge the Gordon and Betty Moore Foundation and the Beckman Institute for their generous support of the Molecular Observatory at Caltech and the staff at Beamline 12–2,

Stanford Synchrotron Radiation Lightsource (SSRL), for their assistance with data collection. Use of the SSRL, SLAC National Accelerator Laboratory, is supported by the U.S. Department of Energy, Office of Science, Office of Basic Energy Sciences under Contract No. DE-AC02-76SF00515. The SSRL Structural Molecular Biology Program is supported by the DOE Office of Biological and Environmental Research, and by the National Institutes of Health, National Institute of General Medical Sciences (including P41GM103393). This project benefited from the use of instrumentation made available by the Caltech Environmental Analysis Center. This work was supported in part by NIH GM045162.

Bibliography

1. Linton KJ, Higgins CF. MicroGenomics The *Escherichia coli* ATP-binding cassette (ABC) proteins. *Mol Microbiol*. 1998; 28:5-13.

2. Rees DC, Johnson E, Lewinson O. ABC transporters: the power to change. *Nat Rev Mol Cell Biol*. 2009; 10(3):218-227. doi:10.1038/nrm2646.

3. Higgins CF. ABC transporters: from microorganisms to man. *Annu Rev Cell Biol*. 1992; 8:67-113. doi:10.1146/annurev.cb.08.110192.000435.

4. Kadaba NS. The high-affinity *E. coli* methionine ABC transporter: structure and allosteric regulation. *Science*. 2008; 321:250-253. doi:10.1126/science.1157987.

5. Locher KP. Mechanistic diversity in ATP-binding cassette (ABC) transporters. *Nat Struct Mol Biol*. 2016; 23(6):487-493. doi:10.1038/nsmb.3216.

6. Jardetzky O. Simple allosteric model for membrane pumps. *Nature*. 1966; 211(5052):969-970. doi:10.1038/211969a0.

7. Widdas WF. Inability of diffusion to account for placental glucose transfer in the sheep and consideration of the kinetics of a possible carrier transfer. *J Physiol*. 1951; (118):23-39.

8. Oldham ML, Khare D, Quiocho FA, Davidson AL, Chen J. Crystal structure of a catalytic intermediate of the maltose transporter. *Nature*. 2007; 450:515-522. doi:10.1038/nature06264.

9. Oldham ML, Chen J. Crystal Structure of the Maltose Transporter in a Pretranslocation Intermediate State. *Science*. 2011; 1202(2011):1202-1205. doi:10.1126/science.1200767.

10. Korkhov VM, Mireku S a, Locher KP. Structure of AMP-PNP-bound vitamin B12 transporter BtuCD-F. *Nature*. 2012; 490(7420):367-372. doi:10.1038/nature11442.

11. Hollenstein K, Dawson RJP, Locher KP. Structure and mechanism of ABC transporter proteins. *Curr Opin Struct Biol*. 2007; 17(4):412-418. doi:10.1016/j.sbi.2007.07.003.

12. Hvorup RN, Goetz B a, Niederer M, Hollenstein K, Perozo E, Locher KP. Asymmetry in the structure of the ABC transporter-binding protein complex BtuCD-BtuF. 2007; 317:1387-1390. doi:10.1126/science.1145950.

13. Oldham ML, Chen S, Chen J. Structural basis for substrate specificity in the *Escherichia coli* maltose transport system. *Proc Natl Acad Sci U S A*. 2013; 110(45):18132-18137. doi:10.1073/pnas.1311407110.

14. Bao H, Duong F. Discovery of an auto-regulation mechanism for the maltose ABC transporter MalFGK2. *PLoS One*. 2012; 7(4):e34836.

doi:10.1371/journal.pone.0034836.

15. Goudsmits JMH, Jan Slotboom D, van Oijen AM. Single-molecule visualization of conformational changes and substrate transport in the vitamin B12 ABC importer BtuCD-F. *Nat Commun*. 2017; 8(1):1652. doi:10.1038/s41467-017-01815-7.

16. Kadaba NS, Kaiser JT, Johnson E, Lee A, Rees DC. The high affinity *E. coli* methionine ABC transporter: structure and allosteric regulation. *Science*. 2008; 321(5886):250-253. doi:10.1126/science.1157987.The.

17. Johnson E, Nguyen PT, Yeates TO, Rees DC. Inward facing conformations of the MetNI methionine ABC transporter: Implications for the mechanism of transinhibition. *Protein Sci*. 2012; 21(1):84-96. doi:10.1002/pro.765.

18. Kadner RJ. Regulation of methionine transport activity in *Escherichia coli*. *J Bacteriol*. 1975; 122(1):110-119.

19. Yang JG, Rees DC. The Allosteric Regulatory Mechanism of the *Escherichia coli* MetNI Methionine ATP Binding Cassette (ABC) Transporter. *J Biol Chem*. 2015; 290(14):9135-9140. doi:10.1074/jbc.M114.603365.

20. Lewinson O, Lee AT, Locher KP, Rees DC. A distinct mechanism for the ABC transporter BtuCD – BtuF revealed by the dynamics of complex formation. *Nat Publ Gr*. 2010; 17(3):332-338. doi:10.1038/nsmb.1770.

21. Nguyen PT, Li QW, Kadaba NS, Lai JY, Yang JG, Rees DC. The contribution of methionine to the stability of the *Escherichia coli* MetNIQ ABC transporter-substrate binding protein complex. *Biol Chem*. 2015; 396(9-10):1127-1134. doi:10.1515/hsz-2015-0131.

22. Kadner RJ, Watson WJ. Methionine Transport in *Escherichia coli*: Physiological and Genetic Systems Methionine Transport in *Escherichia coli*: Physiological and Genetic Evidence for Two Uptake Systems. *J Bacteriol*. 1974;119(2):401-409.

23. Zhang Z, Feige JN, Chang AB, et al. A transporter of *Escherichia coli* specific for L- and D-methionine is the prototype for a new family within the ABC superfamily. *Arch Microbiol*. 2003;180(2):88-100. doi:10.1007/s00203-003-0561-4.

24. Kadner RJ. Transport and utilization of D-methionine and other methionine sources in *Escherichia coli*. *J Bacteriol*. 1977;129(1):207-216.

25. Studier FW. Protein production by auto-induction in high density shaking cultures. *Protein Expr Purif*. 2005;41(1):207-234. doi:10.1016/j.pep.2005.01.016.

26. Strong M, Sawaya MR, Wang S, Phillips M, Cascio D, Eisenberg D. Toward the structural genomics of complexes: Crystal structure of a PE/PPE protein complex from *Mycobacterium tuberculosis*. *Proc Natl Acad Sci*. 2006;103(21):8060-8065. doi:10.1073/pnas.0602606103.

27. Adams PD, Grosse-Kunstleve RW, Hung LW, et al. PHENIX: Building new software for automated crystallographic structure determination. *Acta Crystallogr Sect D Biol Crystallogr*. 2002;58(11):1948-1954. doi:10.1107/S0907444902016657.

28. Dimaio F, Echols N, Headd JJ, Terwilliger TC, Adams PD, Baker D. Improved low-resolution crystallographic refinement with Phenix and Rosetta. *Nat Methods*. 2013;10(11):1102-1106. doi:10.1038/nmeth.2648.

29. Collaborative Computational Project N 4. The CCP4 suite: programs for protein crystallography. *Acta Crystallogr D Biol Crystallogr*. 1994;50(Pt 5):760-763. doi:10.1107/S0907444994003112.

30. Emsley P, Cowtan K. Coot: Model-building tools for molecular graphics. *Acta Crystallogr Sect D Biol Crystallogr*. 2004;60(12 I):2126-2132. doi:10.1107/S0907444904019158.

31. Gouridis G, Schuurman-wolters GK, Ploetz E, et al. Conformational dynamics in substrate-binding domains influences transport in the ABC importer GlnPQ. 2015;22(1). doi:10.1038/nsmb.2929.

CHAPTER 3

AN UNCONVENTIONAL MECHANISTIC MODEL FOR THE *ESCHERICHIA COLI* TYPE-I METHIONINE ABC TRANSPORTER

3.1. Introduction

A methionine transporter is a highly-conserved bacterial ABC importer that consists of four typical subunits: two transmembrane subunits (MetI) that form a translocation pathway, and two nucleotide-binding subunits (MetN) that use the energy from ATP binding and hydrolysis to fuel transport [1–4]. An ABC importer requires an additional component, a substrate-binding protein (SBP), located in the periplasm of Gram-negative bacteria or tethered to the membrane in Gram-positive bacteria and archaea, to deliver substrates to their cognate transporters. For the methionine transporter, the methionine-binding protein, MetQ, serves as the substrate-binding protein [5,6]

The transport mechanism of the methionine transporter is best described by the alternating access model [7,8], in which the transport cycle interconverts between an inward-facing conformation that opens the translocation pathway to the cytoplasm, and an outward-facing conformation that opens it to the periplasm. Structures of transporters in complex with their binding proteins [9–14] have been instrumental in defining the basic features of the transport cycle. The two best characterized ABC importers are the type I (small transmembrane subunits, 5-8 helices per subunit) maltose uptake system, $MalFGK_2$, and the type II (large transmembrane subunits, 10 helices per subunit) vitamin B_{12} uptake system, BtuCD. Structural studies on these importers have provided two renowned

mechanistic models for the transport cycles of type I and type II ABC transporters, although recently they have been challenged by biochemical and single molecule studies [15,16]. Bao and Duong [15] showed that the apo form of maltose-binding protein binds to nanodisc-incorporated maltose transporters with high affinity, and that this complex facilitates the acquisition of maltose into the translocation pathway. In addition, single molecule studies on proteoliposome-incorporated vitamin-B12 transporters, Goudsmits et. al. also pointed out that apo binding protein BtuF forms a stable complex with the BtuCD transporter at a ground state in the absence of ATP and substrate [16]. Substrate is caught by the BtuCD-complexed BtuF, and then shuttled inside the translocation pathway [16].

Although the methionine transporter belongs to type I ABC transporter family, previous works revealed unique features, which include (1) the C-regulatory (C2) domains [17,18] and trans-inhibition regulation, in which binding of L-methionine to these domains inhibit transport and ATPase activity [19,20], (2) the low binding affinity of substrate-bound (holo) MetQ for ATP-free MetNI ($K_d \sim 10^{-4}$ M) (Lewinson, Lee, Locher, & Rees, 2010) and ATP-loaded MetNI ($K_d \sim 1.1$ μM) [22], and (3) the high affinity of substrate-free (apo) MetQ for ATP-loaded MetNI ($K_d \sim 27$ nM) [22].

Currently, only the IWF conformation of MetNI has been solved crystallographically [17,18]. To build a comprehensive model for MetNI transport, we have solved a 2.95Å resolution crystal structure of the ATPγS-bound MetNIQ complex in a catalytic intermediate state. The structure sheds light on the mechanism of the methionine transporter and its regulation by trans-inhibition. In addition, this structure also reveals unexpected features of the binding protein MetQ in complexed form. Coupling structural

and functional characterization of the MetNI methionine transporter, we propose an unconventional mechanistic model for type-I methionine ABC transporter.

3.2. Results and Discussion

3.2.1. Overall architectures of the MetNIQ complex in the outward-facing conformation

We determined a 2.95Å resolution crystal structure of the methionine-ABC transporter, MetNI, in complex with its substrate-binding protein, MetQ (Fig3.1a). Significant conformational changes of MetNI subunits are observed, relative to the uncomplexed MetNI (Fig 3.1a). Superimposition of one MetI subunit of the OWF (shown in pale green) to that of the IWF conformation (shown in gray) (PDB: 3TUI) reveals a rotation of about 31^{o} along the rotation axis, shown in red (Fig 3.11). This rotation results in a large movement of the opposite subunit in a shift of approximately 15Å as a whole rigid body, opening the translocation pathway toward the periplasm (Fig 3.1b).

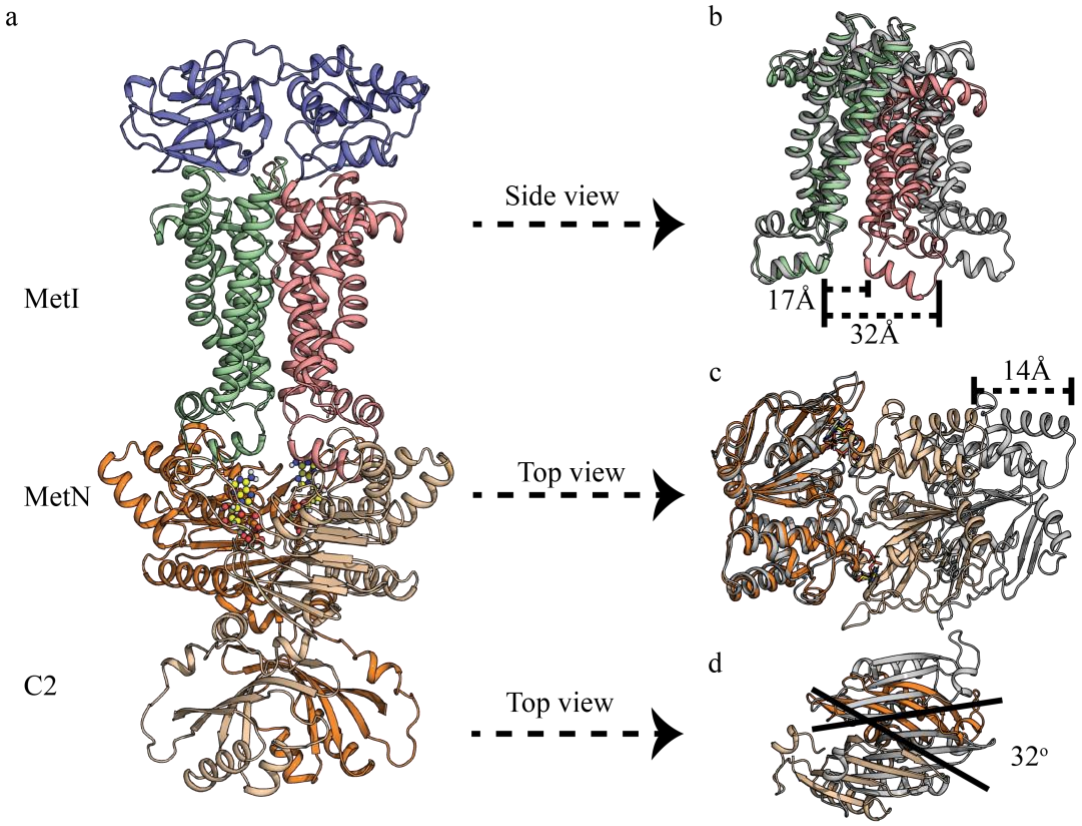

Figure 3.1. Structure of MetNIQ complex. (a) side-view representation of the MetNIQ. MetQ subunit is colored state, MetI subunits pale green and salmon, and MetN subunits tv_orange and wheat, C-regulatory (C2) domains are at the C-termini of MetN subunits. a, c, d, conformational changes of the transmembrane MetI subunits (b), the nucleotide-binding MetN subunits (c), and the C2 domains (d) between their outward-facing (OWF) (colored as described in (a)) and inward-facing (IWF) conformation (colored in gray). One subunit of MetI (pale green) or MetN (tv_orange) of the OWF conformation was overlaid to that of the IWF conformation to highlight the differences in the relative placement of the opposite subunit (b), (c). Superimposition of MetNIQ and MetNI reveals the rotation of the C2 domains (d).

To visualize the movements of the nucleotide-binding domains of the MetN subunits from the IWF to OWF conformation, the two halves of the transporter (MetN, MetI) from the two conformations (PDBs: 6CVL and 3TUI) were superimposed using the transmembrane domain as a fixed domain. As a result, the NBD rotates about 18^{o} along the rotation axis, shown in magenta (Fig 3.11) relative to that in its IWF to adopt its new OWF conformation. The distance between the two nucleotide-binding domains is reduced by about 14Å (Fig 3.1c), some of which allows dimerization of two NBDs in the presence of ATPγS. At the C2 domains, unlike those of the maltose transporter, a twist with an angle of 32^{o} (Fig 3.1d) along the rotation axis, shown in yellow (fig3.11) was observed between this structure and the DM solubilized MetNI (PDB: 3TUJ) [18]. This unique feature is possibly involved in the trans-inhibition event. Our previous work showed that binding of L-methionine to the C2 domains locked the NBDs into the inward-facing conformation [18]. In this L-methionine-bound, IWF/inhibited conformation [18], an L-methionine substrate from one C2 domain forms hydrogen bonds with the other substrate at the interface β-sheet, stabilizing the inward-facing conformation of the transporter (Fig 3.6a). In contrast, the OWF configuration shows a repositioning of the C2 domains by a register shift of the hydrogen bonding network between the two intermolecular β-sheets (A299 – A299 in the IWF to A299 – M301 in the OWF) (Fig3.6c, d). This flexibility of the C2 domains results in the dimerization of MetN subunits in the presence of ATP.

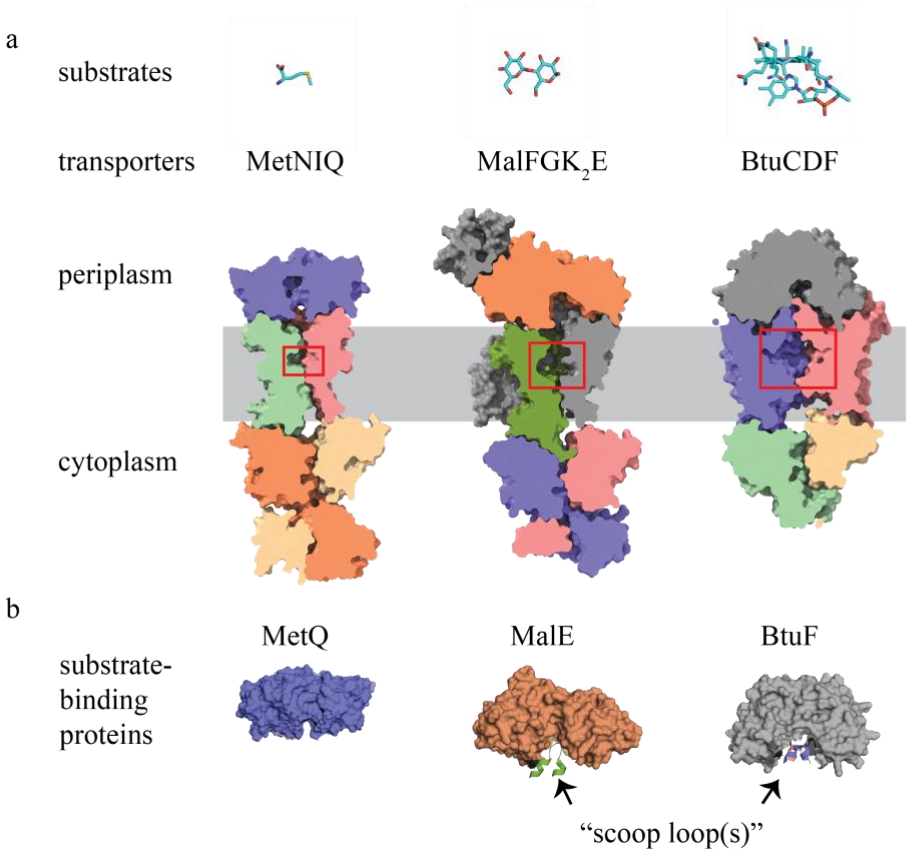

Figure 3.2. Translocation pathways of different ABC importers at a glance. a, Surface slab views of the outward-facing conformations of three ABC importers, including MetNIQ (unpublished), MalFGK2 (PDB: 2R6G), and BtuCDF (PDB: 4FI3), reveal potential substrate-binding pockets (red box) with different sizes and shapes at the translocation pathways. While MetI subunits form a small cavity, larger cavities are observed in the case of maltose and vitamin-B12 transporters. Only maltose (shown in ball and stick) was structurally observed in the cavity. b, Potential different mechanisms of substrate delivery were observed in the three ABC importers mentioned in a. While "scoop loop" was

proposed for substrate handing between the maltose-, and vitamin-B12-binding proteins to their transporters, no "scoop loop" was found in the methionine transporter

3.2.2. Unexpected features of MetQ in complex with MetNI indicate new substrate delivery mechanism

Structures of the maltose (PDB: 2R6G) [11] and vitamin-B12 (PDB: 4FI3) [10] transporters revealed insertion loops, aka "scoop loops", from the transmembrane subunits into the substrate cavities of the binding proteins that facilitate substrate hand-off (fig3.2b). No such scoop loop was found in the MetNIQ complex (fig3.2b). This may indicate that another substrate hand-over mechanism is involved.

The crystal structure of the MetQ in complex with the MetNI transporter (complexed MetQ), (reported here) reveals a conformation distinct from the substrate-free (apo) (reported here) and substrate-bound (holo) (PDB: 4YAH) conformation (fig 3.3a, b). Superimposition of the open (apo) to the complexed MetQ structure shows a 44^{o}-angle hinge-type rotation between two lobes of MetQ (fig3.3a, fig3.11). On the other hand, a 24^{o}-angle twist twofold axis (fig3.3b, fig3.11) was found in the complexed form compared to the holo form of MetQ with an rmsd of 4.4 Å. This distortion is larger than that of the maltose-binding protein, MalE (rmsd=0.7 Å) and of the vitamin-B12 binding protein, BtuF (rmsd=1.0 Å). We suspect that this distortion, together with the small size of the methionine substrate, may allow methionine to access not only the MetQ binding cavity but also the MetNIQ translocation pathway (fig 3.4).

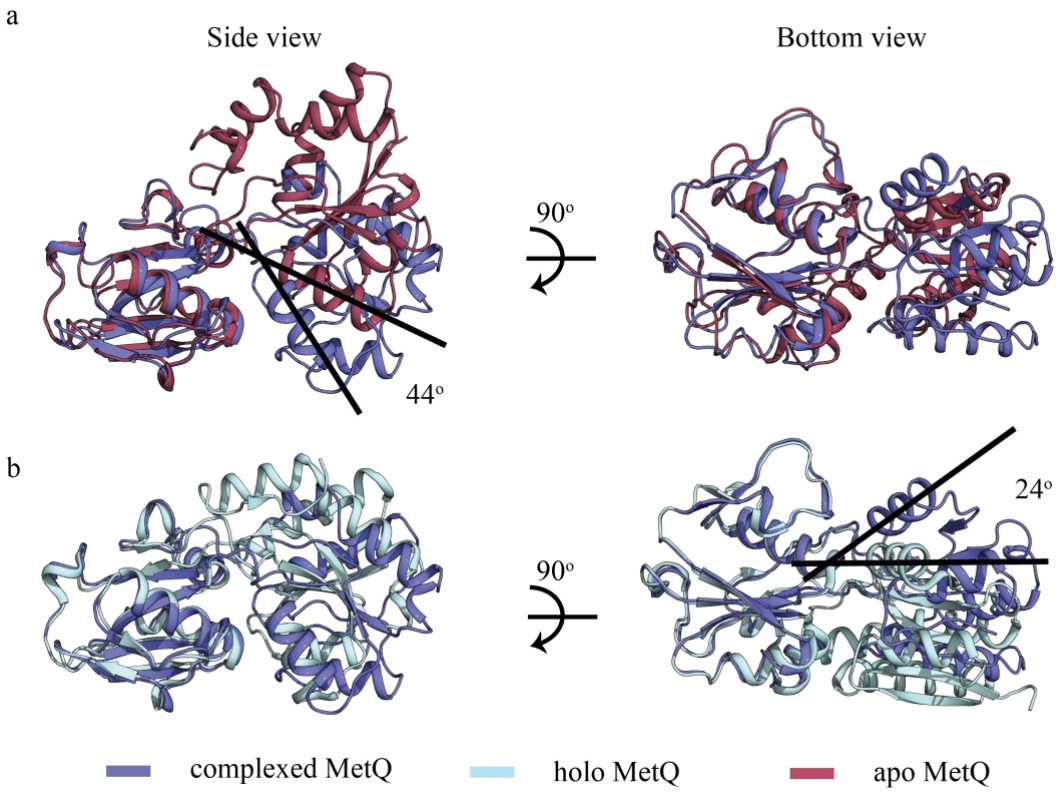

Figure 3.3. An unexpected third conformation of MetQ in complex with MetNI. The crystal structure of MetQ subunit in complex with MetNI (complexed MetQ) (colored state) shows another distinct conformation different from the substrate-free (apo) (colored raspberry) and substrate-bound forms (holo) (colored cyan). Superimposition of the apo and complexed MetQ shows a typical "hinge-type" rotation with a rotation angle of 42°, while a twist 24° was observed along a different axis in the superimposition of the complexed versus holo MetQ (b).

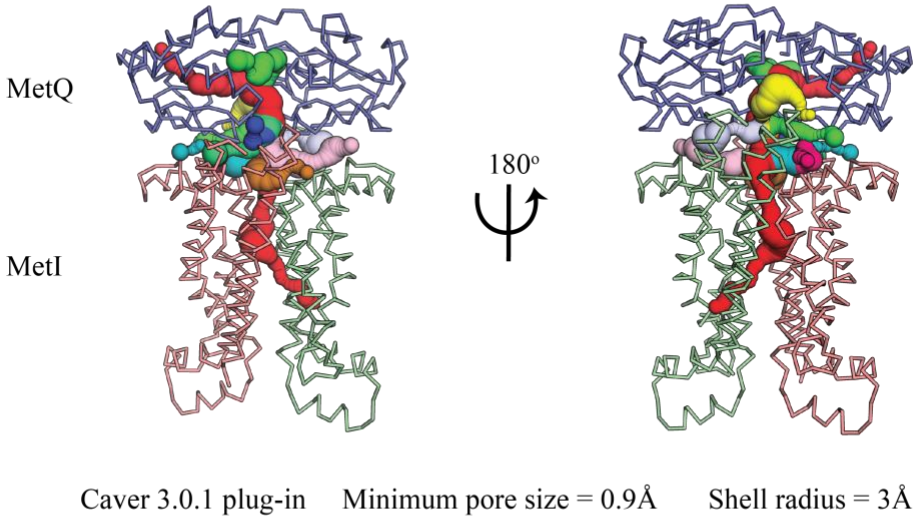

Figure 3.4. Potential substrate pathways for the MetNIQ complex. A twisted conformation of the MetQ in complex with MetNI results in wide open cavities, which are accessible for different substrate pathways shown as surface representations. These pathways were calculated by CAVER 3.0.2 pymol plugin.

3.2.3. Substrate cavity and gating mechanism

Rearrangements of the cytoplasmic and periplasmic gates were observed in the MetNIQ crystal structure (fig3.5a). At the periplasmic gate, residues Y177 and M163 move away from the center of the translocation pathway, compared to those in the IWF conformation of MetNI (Fig3.5b, c). On the other hand, residues M107 (TM3) from both

MetI subunits form a cytoplasmic gate, the bottleneck of the translocation pathway (Fig 3.5d, e).

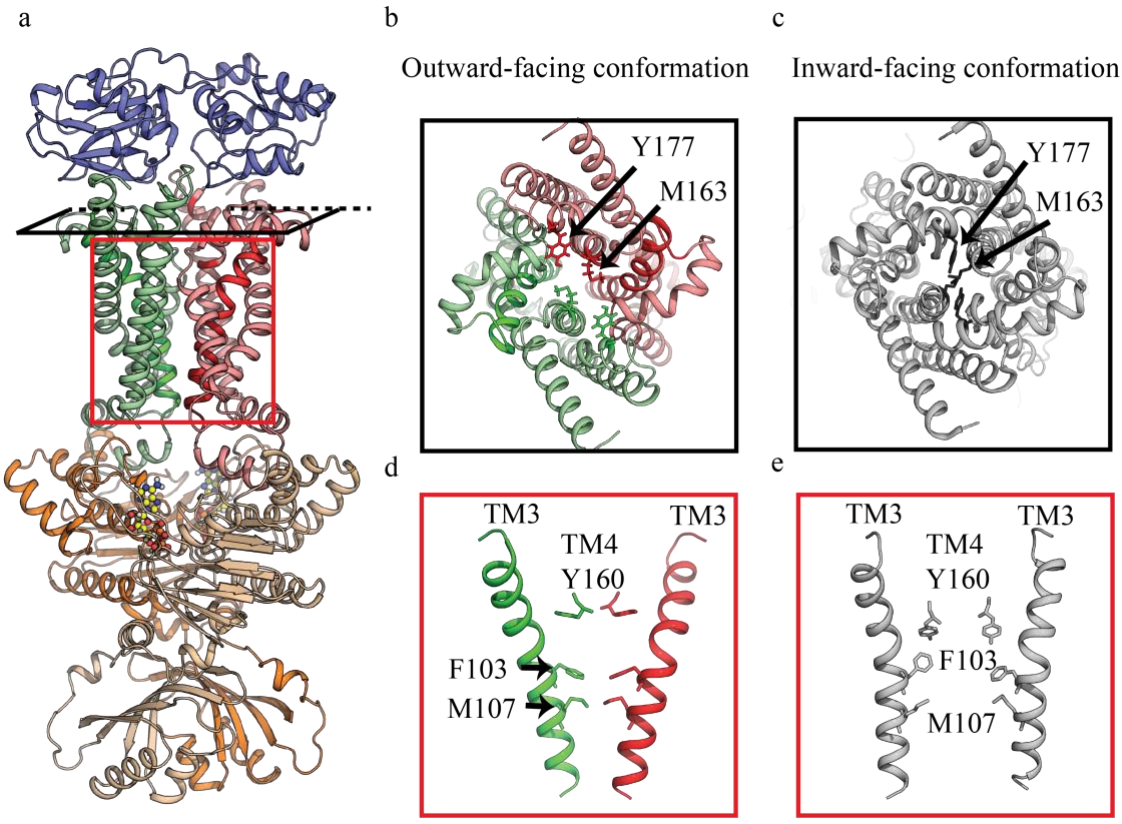

Figure 3.5. Conformational changes of the cytoplasmic, periplasmic gates and C2 domains of the MetNIQ complex. a,b, Structure comparison of the MetI subunits in their outward-facing conformation (colored pale green and salmon) (left boxes) versus inward-facing conformation (colored white and gray) (right boxes) reveals major rearrangements of the periplasmic gate residues, including Y177 and M163 (a), and of the cytoplasmic gate residues, including F103, M107, and Y160 (b).

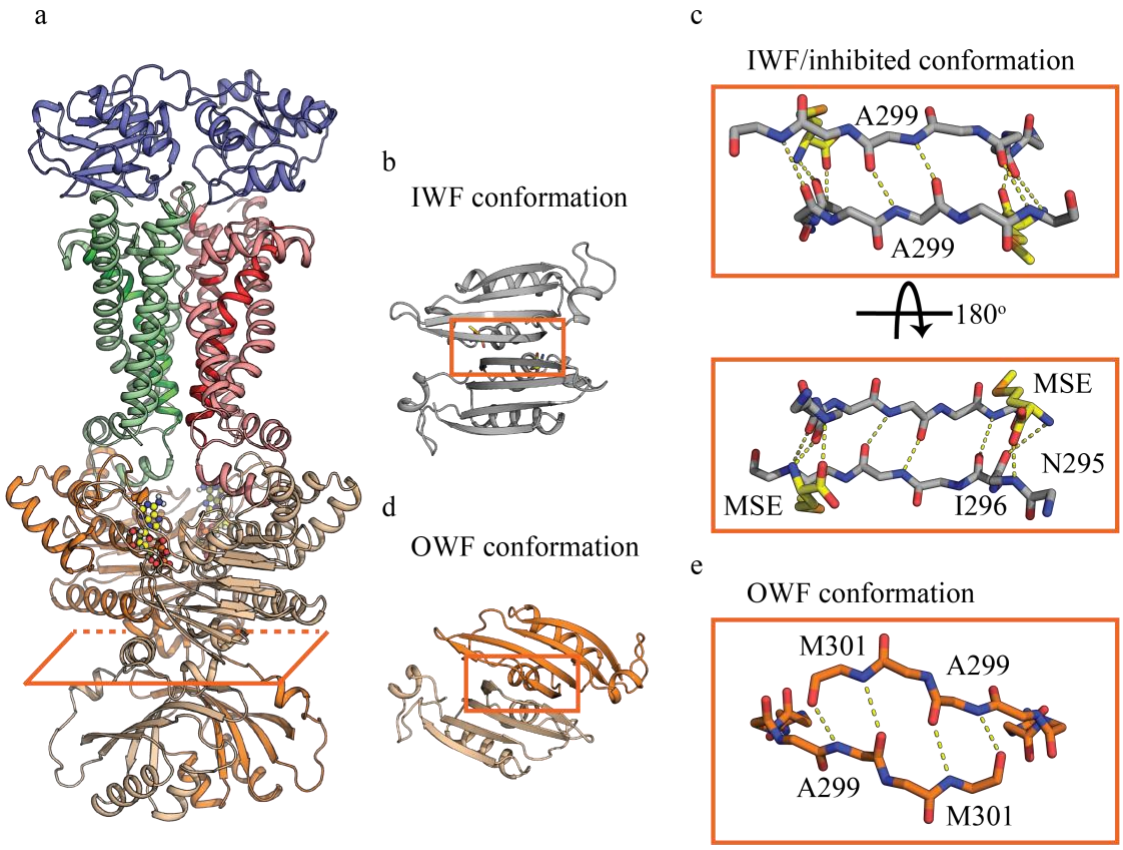

Figure 3.6. Hydrogen-bonding shifts at the interface of C2 domains. Top-down view (d, e) of the C2 domains of the outward-facing conformation MetNIQ (OWF conformation) reveals shifts in hydrogen-bonding network (yellow dashes) A299 – M301, compared to that of the inward-facing conformation MetNI (b, c) (IWF/inhibited conformation), A299 – A299 between 2 β-sheets (shown in ball-and-stick representations) at the domains' interface. Binding of L-semethionine (MSE) at the C2 domains stabilizes the A299 – A299 hydrogen bond, and consequently locks the MetNI in its inward-facing conformation (PDB: 3TUZ).

Rearrangements of the MetI subunits in the OWF conformation create a small cavity (fig3.2a), whose boundary is defined by residues Y160 and F103 at the top and bottom of the cavity respectively (fig3.5b), along the translocation pathway of the MetNIQ. Compared to the known substrate cavities, in the maltose and vitamin-B12 transporters [11,13], this cavity is the smallest one, and proportional to the size and shape of the transported methionine substrate (fig3.2a). We didn't find any methionine binding site in the translocation pathway of MetNIQ either structurally after crystal soaking or biochemically by isothermal calorimetry (ITC) measurement. This differs from the maltose transporter that maltose is found in the translocation pathway [11]; the presence of vitamin-B12 in the translocation pathway has also been inferred biochemically [13]. Interestingly, in MetNIQ, Y160, F103, and M107 residues from both subunits line the translocation pathway as if to form a "selectivity filter" for methionine selection (Fig3.5b). Aromatic rings from these residues may favor a selection toward the sulfur atom of the methionine residue.

3.2.4. The effects of L-methionine to complex formation and stability of MetNIQ complex

L-methionine was shown to inhibit the ATPase activity of MetNI, possibly by binding to the C2 domain and preventing MetN subunits from associating and hydrolyzing ATP [17–19]. As a consequence, this binding event may inhibit complex formation. We sought to reveal the effect of L-methionine on the complex formation of MetNIQ. MetNI was pre-incubated with L-methionine at different ratios (1: 0 to 1: 100, MetNI: L-methionine) and mixed with apo MetQ (N229A) in the presence of ATP-EDTA to form the complex. These reactions were then separated by gel filtration to purify potential MetNI(Q) peaks, and analyzed by SDS-PAGE (Fig 3.7a). MetNIQ complex formation was inhibited by the

presence of L-methionine at a ratio of 1: 10 (MetNI: L-methionine) or higher (Fig 3.7b), suggesting that binding of L-methionine to the C2 domains prevents the stable association of MetNI with MetQ. To test whether L-methionine can destabilize preformed MetNIQ complexes, we set up another set of reactions in which the pre-formed MetNIQ was mixed with L-methionine at different ratios. SDS-PAGE analysis of the MetNIQ peaks showed that the complex largely remains intact at the tested ratios (1: 0 to 1: 100, MetNIQ: L-methionine) (Fig 3.7c).

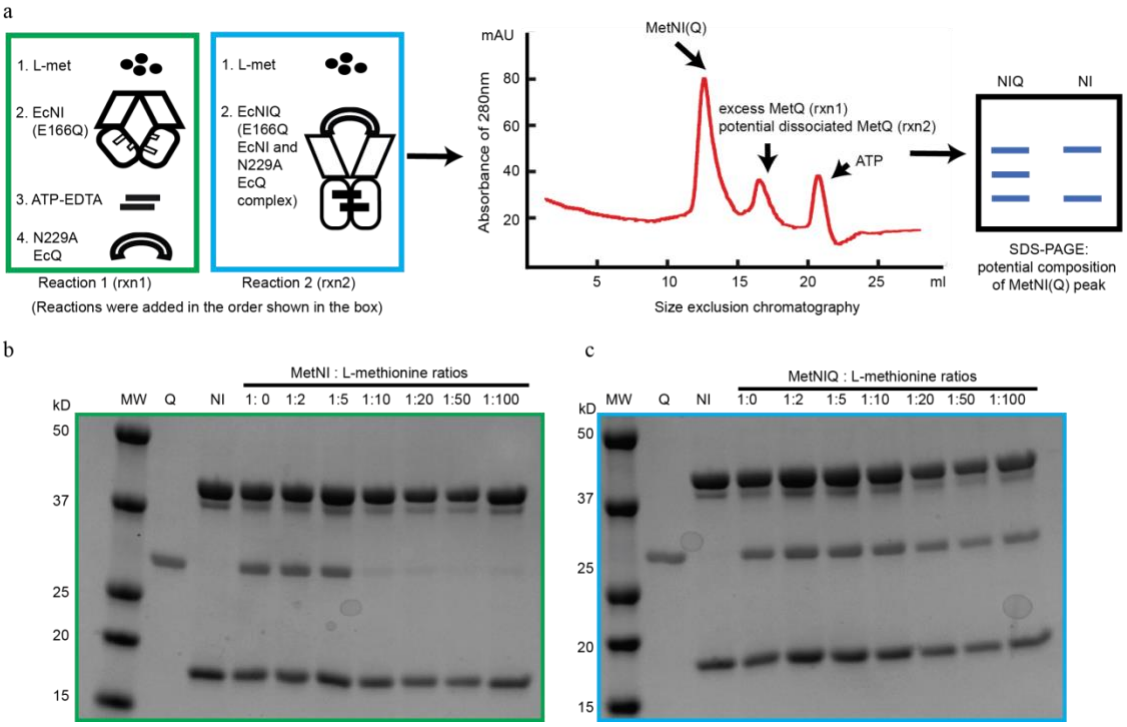

Figure 3.7. The effects of L-methionine on MetNIQ complex formation and stability. a, Experimental setup to observe complex formation or dissociation in the presence of L-methionine. In reaction 1, L-methionine pre-incubated MetNI (E166Q) at different ratios was mixed with MetQ (N229A) in the presence of ATP-EDTA for complex formation, which was detected by gel filtration and SDS-PAGE. In reaction 2, pre-formed MetNIQ complex was incubated with L-methionine at different ratios, and complex dissociation assessed by

gel filtration and SDS-PAGE. SDS-PAGE results of the MetNI(Q) peaks from gel filtration of the set of reactions #1 (b) show inhibition of MetNIQ complex formation by L-methionine (b) at a ratio of 1: 10 (MetNI: L-methionine). This indicates that binding of L-methionine locks the MetNI in its inward-facing conformation, preventing MetN subunits from dimerization; however, the preformed MetNIQ complex is stable in the presence of L-methionine at a highest tested ratio of 1: 100 (MetNIQ : L-methionine) (c)

3.2.5. Functional characterization of the MetNI methionine transporter confirms new roles of the binding protein MetQ

Transport assays of the methionine transporter and its mutants were performed in vivo using a ΔmetNIQ-knockout *E. coli* strain. It is known that there are two transport systems in *E coli* that are responsible for methionine uptake [23]. One is the MetNIQ transport system (MetD operon) and the other is an uncharacterized MetP [6]. While MetD can transport both L- and D-isomers of methionine, MetP can only transport L-methionine [6,23,24]. To selectively study MetNI transport, we took advantage of its unique feature of D-methionine transport and used a D-methionine derivative, namely D-selenomethionine, as the transport substrate for quantification by ICP-MS (Fig3.8a). Kinetic constants for the transport activity of D-selenomethionine derived from Michaelis-Menten analysis (Fig3.8b) are shown in Table 1. The maximal uptake rate of the wild-type MetNIQ is 6.3 ± 0.4 nmol/min/mg of transporter (n=6) (Fig 3.8b). Since L-methionine is present in the cytoplasm at 0.1 – 0.3 mM, to bypass the potential transinhibition effect, a N295A mutation at the C2 domain of the MetNI was made to abolish its binding to L-methionine (table 3.2). This mutant results in a higher uptake rate of 10 ± 0.5 nmol/min/mg of transporter (n=12). A deletion of MetQ yields a poor maximal transport rate of 0.2 ± 0.1 nmol/min/mg of

transporter (n=3), which indicates that MetQ is necessary for the transport; however, an unanswered question is whether MetQ binds and delivers methionine substrate to the transporter. To address this question, we generated a substrate-binding deficient N229A mutation that lowers the affinity of MetQ to D-selenomethionine by 10-fold (table 3.2). It was unexpected that the N229A MetNIQ mutation stimulates the maximal transport rate for D-selenomethionine (V_{max}=10.5 ± 0.9 nmol/min/mg of transporter) (n=6) by almost 1.5 fold compared to the wt MetNIQ (V_{max}=6.3 ± 0.4 nmol/min/mg of transporter) (table 3.1). A similar stimulation is observed for the N229A mutation of N295A MetNIQ (V_{max}=15.4 ± 1.3 nmol/min/mg of transporter) (n=6) compared to the N295A MetNIQ (V_{max}=10 ± 0.5 nmol/min/mg of transporter) (fig3.8b and table 3.1). We hypothesize that binding protein is required to stabilize the OWF conformation of MetNI for substrate loading. This hypothesis is in agreement with the fact that apo MetQ has a higher binding affinity toward ATP-loaded MetNI (K_d ~ 27 nM), but lower to D-selenomethionine (K_d ~7 μM). Hence, the apo MetQ binds and stabilizes the OWF-conformation MetNI, some of which opens up a translocation pathway for the substrate loading (fig 3.4). At low concentrations of substrate, the wild-type (wt) binding protein may recruit substrate to the complex, as indicated by a faster transport rate at the lower concentrations of substrate with K_M ~1.8 μM for wt MetNIQ and K_M ~1.7 μM for N295A MetNIQ (table 3.2), in compared to higher K_M observed for the substrate-binding deficient mutants (N229A) for MetNIQ and N295A MetNIQ with K_M values ~7.4 μM and 4.8 μM, respectively (fig3.8b, table 3.1).

Mutation of either of the two cytoplasmic gating residues to alanine (F103A, M107A) results in no transport activity *in vivo* (Fig3.8b, table 1), possibly due to obstruction of the translocation pathway by non-selected, nonspecific molecules in the

periplasm. In contrast, the Y160A mutation results in a gain-of-function mutant, and increases the uptake rate by two-fold (V_{max}= 14 ± 1.3 nmol/min/mg of transporter) compared to that of N295A MetNIQ (V_{max}= 10 ± 0.5 nmol/min/mg of transporter). The removal of the upper gating residues by Y160A mutation could make the translocation more accessible for substrates to get loaded in.

Table 3.1. Summary of kinetic constants for transport activity of MetNIQ variants. The maximum uptake rate (V_{max}) and Michaelis-Menten constant (K_m) were determined from the plot shown in fig3.8. N/A: not applicable; - not detectable.

MetNIQ variants	Uptake rate V_{max} (nmol/min/mg of transporter)	K_m (μM)
MetNIQ	6.3 ± 0.4	1.8 ± 0.4
MetNI	0.2 ± 0.1	N/A
N295A (EcN) MetNIQ	10 ± 0.5	1.7 ± 0.3
N229A (EcQ) MetNIQ	10.5 ± 0.9	7.4 ± 0.5
N295A, N229A MetNIQ	15.4 ± 1.3	4.8 ± 0.7
N295A, F103A (EcI) MetNIQ	-	-
N295A, M107A (EcI) MetNIQ	-	-
N295A, Y160A (EcI) MetNIQ	14 ± 1.3	4.1 ± 0.2

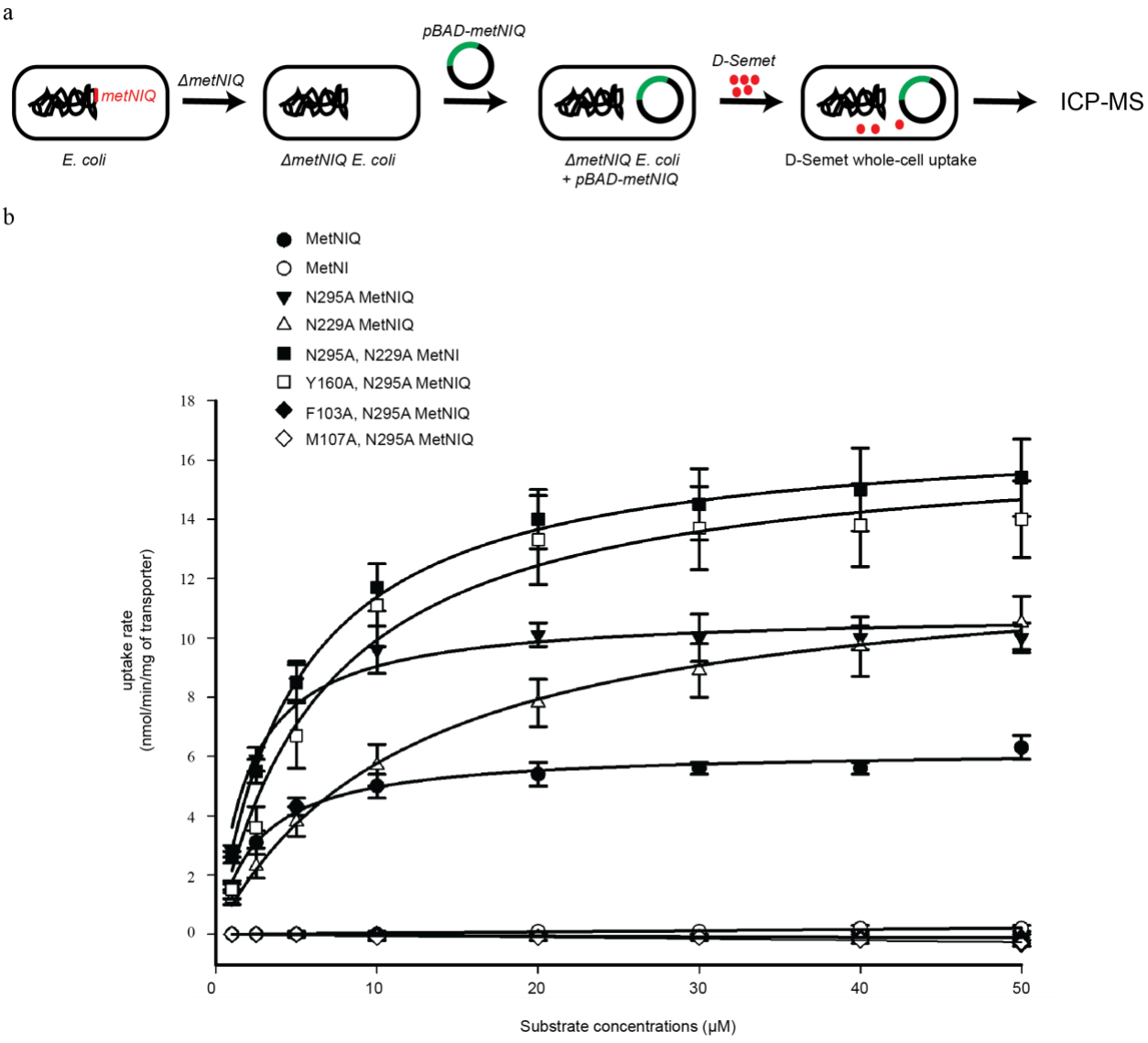

Figure 3.8. In vivo uptake of MetNIQ and its variants. a, Schematic of whole-cell uptake assay for MetNIQ variants. b, Michaelis-Menten plot of initial velocities versus substrate concentrations for transport activities of MetNIQ and its variants.

3.2.6. Proposed transport mechanism

The most detailed transport model is built upon structural studies of the maltose transporter [12]. In this model, MalE delivers ligand to the transporter. However, this model

can't explain (1) the low affinity of substrate-bound MetQ to the IWF conformation MetNI, (2) the high affinity of substrate-free MetQ to the ATP-loaded MetNI, and (3) the high uptake rate of the substrate-binding deficient mutant of MetNIQ (N229A). Combining the structural insights with thermodynamic binding constants and enzyme kinetic transport activities, we propose another mechanistic model, illustrated in figure 3.9, to explain the biochemical and structural observations for the methionine transporter. A transport cycle starts with a resting- state L-methionine-free MetNI (PDB: 3TUJ) that can bind two ATPs and acquire the outward-facing conformation MetNI (hypothetical model) (state 2). This hypothetical ATP-bound MetNI conformation was modeled based on knowledge of high basal ATPase activity of MetNI in the presence of ATP [19], as well as a reported crystal structure of AMP-PNP-bound vitamin-B12 transporter trapped by a disulfide bond. The ATP-bound MetNI is transient but stabilized by association of the apo MetQ to form the MetNIQ complex (reported here) (state 3). Methionine can be loaded into the open translocation pathway. Residues Y160, F103, and M107 may form a methionine binding pocket in the translocation pathway. Upon ATP hydrolysis, MetNI adopts its post-hydrolysis ADP-bound inward-facing conformation (PDB: 3TUI), the translocation pathway opens towards the cytoplasm, releasing methionine inside the cell (state 4). The transporter is ready to bind ATP molecules for the next cycle, unless internal L-methionine accumulates to a high concentration in the cell. L-methionine can then bind and lock the C2 domains by stabilizing the A299 –A299 hydrogen bonding networks at the C2 domains' interface, and, in turn, arrest MetNI in its IWF (PDB: 3TUZ) (state 5). This arrested IWF conformation of MetNI is unlocked by the dissociation of L-methionine molecules (fig3.9). The cycle restarts with a resting-state MetNI or an exchange of ADP for ATP for the IWF

MetNI. This mechanistic model can be applied for other Type-I ABC importers, and for other ABC transporters subjected to trans-inhibition.

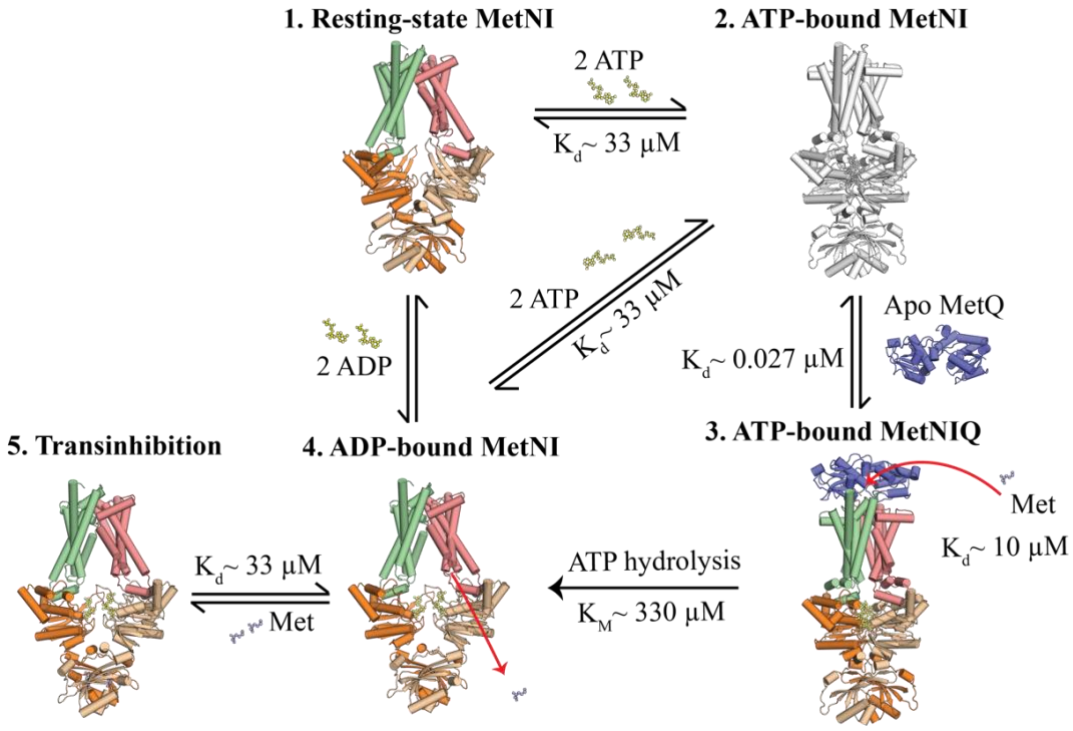

Figure 3.9. Proposed mechanistic atomic model of the methionine-ABC transporter. The states are ordered to demonstrate transport cycle of the methionine transport system, including MetNI and MetQ shown in cylinder diagrams. Methionine, ADP, and ATP are shown as spheres. State 1, 3, 4, 5 represent crystal structures of MetNI(Q), while state 2 is hypothetical model of MetNI based on biochemical evidence of high ATPase activity of MetNI in the absence of MetQ. State 1 represents a resting state of MetNI (PDB: 3TUJ) with no ADP, no L-methionine. State 2 represents an ATP-bound MetNI with dimerized MetN subunits. State 3 represents an ATP-bound MetNI in complex with its binding protein, MetQ reported here. At this state, the L/D-methionine can access the translocation

pathway of the MetNIQ assembly. State 4 represents an ADP-bound MetNI, a post-hydrolysis state of MetNI where 2 ADP molecules bound to the MetN subunits (PDB: 3TUI). Methionine is imported into the cytoplasm upon conformational changes from the OWF to IWF conformation. State 5 represents a trans-inhibition event of MetNI where excess L-methionine in the cytoplasm binds the C2 domains and locks MetNI in its IWF conformation (PDB: 3TUZ).

Table 3.2. Summary of dissociation constants of methionine to MetNI/MetQ. Binding affinities of different methionine isomers and its derivative, selenomethionine were measured by heat exchange from Isothermal Calorimetric experiments. N/A: not applicable, - not detectable.

	Substrates		
Proteins	**L-methionine**	**D-methionine**	**D-selenomethionine**
MetQ	2.3 ± 0.6 nM	7.5 ± 1.9 μM	7.9 ± 1.0 μM
N229A MetQ	340 ± 50 μM	169 ± 4 μM	80 ± 20 μM
MetNI	33 ± 4 μM	N/A	N/A
N295A (EcN) MetNI	-	N/A	N/A
N295A, N229A MetNIQ	-	-	-

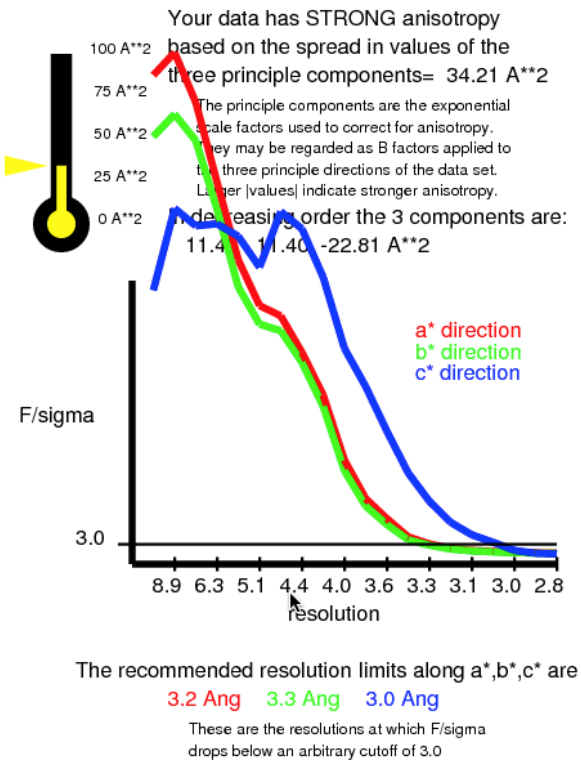

Fig 3.10. Ellipsoidal truncation and anisotropic scaling of strong anisotropic diffraction data. Data observed from a MetNIQ crystal were ellipsoidally truncated and scaled by UCLA MBI Diffraction Anisotropy Server (http://services.mbi.ucla.edu/anisoscale). Data were truncated at the resolution limits along the directions a, b*, and c* to resolution 3.2 Å, 3.3 Å and 3.0 Å respectively, at which F/sigma drops below 3.0.*

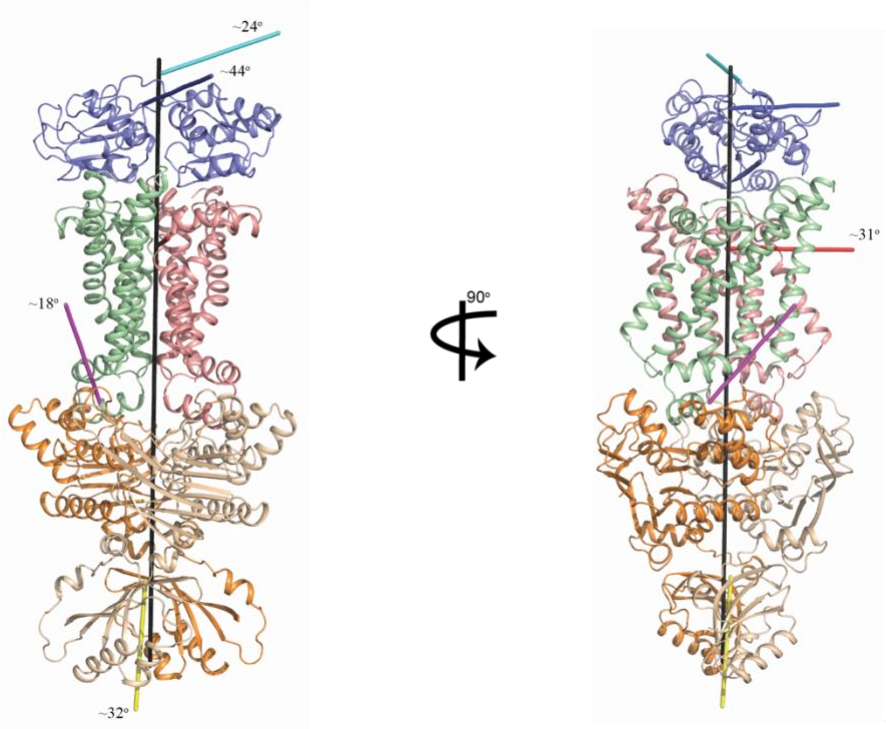

Fig 3.11. Principal component analysis of the methionine structures. Superimposition of individual components of the MetNIQ structure to those of the MetNI and MetQ structures to calculate the rotation axes (depicted as sticks with angles, cyan: complexed MetQ to apo MetQ, blue: complexed MetQ to holo MetQ, magenta: MetN rotation was shown by superimposition of MetI from IWF to OWF conformations to reveal the rotation of MetN of half transporter MetNI) to go from one conformation to the other, yellow: superimposition of the TMDs of MetNI and MetNIQ. Rotation angles were stated as degrees

3.3. Materials and methods

3.3.1. Cloning, expression, and purification

The metN and metI genes were amplified from *E. coli* K12 genomic DNA, and cloned into a pET - modified dual vector, under two T7 promoters (pTN2). The metQ gene

encoded for a mature MetQ with no signal sequence was cloned into a separate pET19b (+) plasmid with N-terminal deca-histidine tag followed by an enterokinase-cleavage site. All of the mutations, including E166Q, N295A in MetN; and N229A in MetQ, were done by site-directed mutagenesis (Stratagene). The cloned plasmids were expressed separately in *E. coli* BL21-gold (DE3) cells (EMD) at room temperature in ZY media [25].

Purification of MetNI mutants was carried out by homogenizing 10 g cell paste in 100 ml of lysis buffer containing 20 mM Tris-HCl pH 8, 100 mM NaCl, 10% glycerol, 5 mM β-mercarptoethanol (βMe), 20 μg/ml DNAseI, 200 μg/ml lysozyme. The cells were broken by three passes through a cell disruptor (M110L pneumatic microfluidizer) (Microfluidics). $C_{12}E_7$ was added at a final concentration of 0.5% (v/v) for solubilizing membrane fractions at 4°C for 2 hours. Unlysed cells and insoluble membranes were removed by centrifugation at 100,000 x g, 4°C, and 30 min. The supernatant was collected, added 70 mM imidazole pH 8.0, and loaded to 5 ml Ni-sepharose HP column (GE Healthcare) that equilibrated with MetNI's purification buffer containing 20mM Tris-HCl pH 7.5, 100 mM NaCl, 0.1% $C_{12}E_7$, 70 mM imidazole. After sample loading, 12 column volumes of the same purification buffer were flowed through to wash non-specific binding to the Ni beads. Two column volumes of MetNI's elution buffer containing 20 mM Tris-HCl pH7.5, 100mM NaCl, 0.1% $C_{12}E_7$, 300 mM imidazole was used to elute protein off the Ni-column. The eluate was then subjected for size-exclusion chromatography. The eluted peaks were collected, concentrated, ultracentrifuged (267,000 x g, 20 min, 4°C) to remove aggregation, and adjusted to 12 mg/ml. 300ul-per-tube aliquots of MetNI was flash frozen by liquid nitrogen (LN2) and stored at -80°C. In preparing MetNI samples for ITC,

buffer containing 20 mM TAPS pH8.5, 100 mM NaCl and 0.025% (w/v) DDM was used for

Purification of mature MetQ was done by resuspending 10 g cell paste in 100ml of lysis buffer as mentioned above. Cell lysis was done by freezing and thawing for 3 cycles in liquid nitrogen (LN_2) and in 42^{o}C- water bath respectively. Clearing of cell lysates was done by centrifugation at 37,500 x g, 30 min, and 4^{o}C. After the supernatant was collected, 70 mM imidazole pH 8.0 before was added before loading onto a 5 ml Ni-sepharose HP column (GE Healthcare) equilibrated with purification buffer containing 20 mM Tris-HCl pH7.5, 100 mM NaCl, 70 mM midazole. After sample loading, 12 column volumes of the same buffer were washed through the column to wash non-specific binding to the Ni beads. Two column volumes of an elution buffer containing 20 mM Tris-HCl pH 7.5, 100 mM NaCl, 300 mM imidazole were used to elute protein off the Ni-column. The eluate was then subjected to size-exclusion chromatography. The eluted peaks were pooled, incubated with enterokinase, light chain (NEB) to cleave the His tag and passed through a hand-packed Ni column again to remove uncut MetQ. The His-tag cleaved MetQ was then concentrated to 20mg/ml and flash-frozen in aliquots of 300 µl per tube. While the *E. coli* N229A MetQ mutant was used for MetNIQ complex formation, the *N. meningitides* N238A MetQ mutant was used for crystallization of an apo MetQ.

3.3.2. Selenomethionine-substituted proteins

To prepare selenomethionine-substituted MetNI and MetQ proteins, the cloned plasmids were transformed in *E. coli* auxotroph B834 (DE3) cells (EMD), which were then grown in PASM media [25], containing 125 µg/ml selenomethionine for 3- 5 days at room temperature.

3.3.3. Crystallization of the *E. coli* MetNIQ protein complex and the apo MetQ

For crystallization of the native MetNIQ and selenomethionine-substituted MetNIQ, the complex formation was described previously. Crystallization screens for MetNIQ was done at different concentrations, from 5- 20 mg/ml, by vapor diffusion in hanging drops at 20^{o}C using 3 different commercial kits, including memgold-2, MORPHEUS (Molecular dimension) and PEGRx (Hampton Research). The MetNIQ was crystallized in reservoirs containing 0.1 M MES pH 6 and 22% PEG 400, using 5 mg/ml protein at a ratio of protein to reservoir 2: 1. Crystals appeared after 2-3 days, fully grew after 5-7 days, and shattered after 10-14 days. Crystals were harvested at day 7 and cryoprotected by increasing PEG 400 concentration to 25% and then 30%, and flash frozen for data collection. Selenomethionine-substituted MetNIQ and MetQ crystals often diffracted better than the native ones.

3.3.4. Heavy-metal derivatives

MetNIQ crystals were soaked in crystallization buffer (0.1M MES pH 6 and 22% PEG 400) containing 1 mM K_2HgI_4 for an hour before back-soaking, cryo-protecting and flash freezing.

3.3.5. Crystallization of the MetQ homolog from *N. meningitides*

We encountered many challenges in crystallizing the *E coli* MetQ in either its apo or holo forms. Consequently, we tested several homologs of *E. coli* MetQ and found MetQ homolog from *Neisseria meningitis* that yielded multiple crystal forms. The apo MetQ (N238A) from *N. meningitis* was crystallized in a condition containing 0.2 M $MgCl_2$, 0.1 M Bis-Tris pH5.5, and 25% PEG3350. Crystals were fully grown after 7 days, and were

cryo-protected by increasing PEG concentration to 35% in increments of 5% and flash-frozen for data collection.

3.3.6. Data collection and structure determination

All X-ray diffraction datasets were collected at the Stanford Synchrotron Radiation Laboratory (SSRL) beamline 12-2 equipped with a PILATUS 6M PAD detectors. Diffraction images were processed and scaled with XDS.

To determine structure of MetNIQ, several datasets diffracting anisotropically to 4 Å – 3 Å resolution were collected at the wavelengths of 1.0000 (native crystals) and 0.09794 (Semet-substituted crystals), respectively. Ellipsoidal truncation and anisotropic scaling were applied to the MetNIQ diffraction datasets using the UCLA MBI Diffraction Anisotropy server (http://services.mbi.ucla.edu/anisoscale) [26] (Fig. 3.10). All crystals belonged to space group $P3_221$ and showed partial twinning with H-alpha twinning fractions ranging from 0.10 to 0.176 determined by Xtriage (Phenix) [27]; therefore, a twin law with operator -h, -k, l was applied. Initial phases were obtained by AutoSol (Phenix) using SAD data from a 3.8 Å -selenomethionine derivative crystal and a $MalFGK_2$-E (PDB: 2R6H) derived model of MetNI in an OWF conformation as a partial model. MR-SAD experimental phasing (Phaser-EP, Phenix) using heavy-atom (selenium) sites was carried out to reduce model bias. These phases are extended to 3.5 Å resolution and later 2.95 Å resolution using two other higher resolution datasets. The latter one showed clear electron densities for MetQ, which allows us to manually dock two individual lobes of MetQ. Additional validation was obtained from the location of mercury sites observed from a K_2HgI_4-soaked MetNIQ crystal that diffracts to 2.95 Å. The MetNIQ model was refined using a combination of Phenix.refine, Rosetta refinement (Phenix) [28], and Refmac5 (CCP4)

[29]. The final model of MetNIQ fits the density for the 2.95Å dataset well with R_{work}/R_{free}= 0.23/0.25.

To determine structure of an apo *N. meningitides* MetQ, a dataset of a selenomethione derivative crystal diffracted to 1.56 Å resolution was collected at the wavelength of 0.9794 Å. The crystal belonged to a space group $P2_12_12$ with cell dimensions of a = 52.56 Å, b = 89.66 Å, c = 45.09 Å. Experimental phasing was performed by Autosol (Phenix) with nine selenomethionine sites. Residues were partially built by Autobuild (Phenix) and manually using Coot [30]. The MetQ model was refined using Phenix.refine (Phenix). The final model of the apo MetQ fits the density with R_{work}/R_{free}= 0.18/0.22.

3.3.7. In vivo transport assays

Whole-cell uptake assays were conducted following an established protocol by the Poolman lab [31]. In brief, different arabinose-inducible (pBAD) plasmids that carry variants of metN, metI, and metQ genes were transformed into ΔmetNIQ *E. coli* strain "BW2115". Cells were grown in LB media to an OD_{600} of 1.5, induced for 2 hr with 0.2% arabinose and harvested by centrifuging for 10 min at 5,000 x g, 4°C. The cell pellets were then washed twice in 50 mM sodium phosphate buffer pH 6.5 and resuspended to OD_{600}~10 in the same buffer. Before transport assays, cells were energized with 0.5% glucose and 5 mM $MgCl_2$ for 10 min at 37°C. The transport assays were started by adding D-selenomethionine at different concentrations at 37 °C, shaking at 300 rpm. The reactions were then stopped by centrifugation at 18,000 x g, 4 °C, for 1 min, followed by discarding the supernatant. The pellet was washed three more times in the same buffer before homogenizing in 20% HNO_3. The samples were incubated at 85 °C overnight and diluted ten fold for quantifying selenium content by inductively coupled plasma mass spectrometry

(ICP-MS) (8800 QqQ, Agilent). The amount of MetNI in each reaction was quantified by western blot using anti-his antibody against His-tagged MetN. A correlation between different substrate concentrations and uptake rate was shown in a final Michaelis-Menten plot (Fig 3.8b) and a summary table (table 3.1). Data were processed using SigmaPlot 10.0 (SigmaPlot).

3.3.8. Qualitative determination of complex formation

Complex formation of MetNIQ and gel filtrations were carried out as described previously (Nguyen et al, 2015 with the minor modification that L-methionine was added at different concentrations relative to the tested ratios of 1: 0 – 1: 100, MetNI(Q): L-methionine in a chronological order that is shown in figure 5a. In brief, complex formation was assessed by mixing E166Q MetNI transporter and its cognate binding protein, MetQ, at a molar ratio of 1: 1.25 (MetNI: MetQ) in the presence of 1 mM ATP and 1 mM EDTA. The mixture was incubated for 1 hour at room temperature and ultracentrifuged at 267,000 x g, 4 ^{o}C for 20 min to remove any aggregation. Samples were injected onto a Superdex S200 10/300 sizing column (GE Healthcare) equilibrated with buffer containing 20 mM TAPS pH 8.5, 100 mM NaCl, 1 mM ATP, 5 mM EDTA, 0.3% Cymal-5. The absorbance reading at 280 nm and the retention volume of the peak were used to follow complex formation. MetNIQ complex formation was verified by analyzing the highest peak by SDS PAGE using any-kD Criterion gels (Bio-Rad). Two independent experiments were conducted per condition.

3.3.9. Isothermal Titration Calorimetry

MetNI, MetNIQ, and MetQ samples were dialyzed overnight in their purification buffers using a Slide-a-lyser mini dialysis device (Thermo Scientific). The samples were

then ultra-centrifuged at 267,000 x g, 4ºC for 20min to remove aggregates and adjusted the concentrations to 100 µM, 100 µM, and 20 µM, respectively. Substrate D-methionine was prepared in the last dialysis buffer of each sample. Titrations of D-methionine to MetNI, MetNIQ, and MetQ samples were done on a MicroCal iTC-200 calorimeter at 25ºC. Data were processed using Origin v7.0 (Origin lab).

Table 3.3. Data collection and refinement statistics for apo MetQ crystal

Protein name	apo NmQ
Wavelength	0.97946
Resolution range	34.22 - 1.559 (1.615 - 1.559)
Space group	P 21 21 2
Unit cell	52.564 89.663 45.088 90 90 90
Total reflections	103820
Unique reflections	30754 (2741)
Multiplicity	6.5(5.4)
Completeness (%)	98.77 (89.75)
Mean I/sigma(I)	10.4(2.4)
Wilson B-factor	17.16
R-merge	0.167(3.329)
R-meas	0.182(3.732)
R-pim	0.071(1.551)
CC1/2	0.995(0.182)
Reflections used in refinement	30752 (2741)
Reflections used for R-free	2000 (179)
R-work	0.1881 (0.2579)

R-free	0.2199 (0.2914)
Number of non-hydrogen atoms	2143
macromolecules	1895
solvent	248
Protein residues	241
RMS(bonds)	0.003
RMS(angles)	0.68
Ramachandran favored (%)	97.49
Ramachandran allowed (%)	2.51
Ramachandran outliers (%)	0.00
Rotamer outliers (%)	0.99
Clashscore	2.66
Average B-factor	25.47
macromolecules	24.52
solvent	32.69
Number of TLS groups	4

Statistics for the highest-resolution shell are shown in parentheses.

Table 3.4. Data collection and refinement statistics for MetNIQ crystal (after ellipsoidal truncation and anisotropic scaling)

Wavelength	1.00582
Resolution range	39.39 - 2.953 (3.058 - 2.953)
Space group	P 32 2 1
Unit cell	107.96 107.96 354.52 90 90 120
Total reflections	

Unique reflections	42966 (526)
Multiplicity	19.3(10.5)
Completeness (%)	83.45 (10.41)
Mean I/sigma(I)	14.7(1.5)
Wilson B-factor	
R-merge	0.196(26.891)
R-meas	0.202(28.291)
R-pim	0.046(10.921)
CC1/2	0.998(0.052)
Reflections used in refinement	42968 (528)
Reflections used for R-free	2174 (29)
R-work	0.2481 (0.3734)
R-free	0.2582 (0.4223)
Number of non-hydrogen atoms	10358
macromolecules	10291
ligands	67
Protein residues	1344
RMS(bonds)	0.012
RMS(angles)	1.61
Ramachandran favored (%)	93.32
Ramachandran allowed (%)	6.38
Ramachandran outliers (%)	0.30
Rotamer outliers (%)	1.60
Clashscore	4.23
Average B-factor	73.96

macromolecules	74.18
ligands	40.31
Number of TLS groups	18

Statistics for the highest-resolution shell are shown in parentheses.

Bibliography

1. Higgins CF. ABC transporters: from microorganisms to man. *Annu Rev Cell Biol*. 1992; 8:67-113. doi:10.1146/annurev.cb.08.110192.000435.
2. Kadaba NS. The high-affinity *E. coli* methionine ABC transporter: structure and allosteric regulation. *Science (80-)*. 2008; 321:250-253. doi:10.1126/science.1157987.
3. Locher KP. Mechanistic diversity in ATP-binding cassette (ABC) transporters. *Nat Struct Mol Biol*. 2016; 23(6):487-493. doi:10.1038/nsmb.3216.
4. Rees DC, Johnson E, Lewinson O. ABC transporters: the power to change. *Nat Rev Mol Cell Biol*. 2009; 10(3):218-227. doi:10.1038/nrm2646.
5. Merlin C, Gardiner G, Durand S, Masters M. The *Escherichia coli* metD Locus Encodes an ABC Transporter Which Includes Abc The *Escherichia coli* metD Locus Encodes an ABC Transporter Which Includes Abc (MetN), YaeE (MetI), and YaeC (MetQ). *Society*. 2002; 184(19):5513-5517. doi:10.1128/JB.184.19.5513.
6. Zhang Z, Feige JN, Chang AB, et al. A transporter of *Escherichia coli* specific for L- and D-methionine is the prototype for a new family within the ABC superfamily. *Arch Microbiol*. 2003; 180(2):88-100. doi:10.1007/s00203-003-0561-4.
7. Widdas WF. Inability of diffusion to account for placental glucose transfer in the sheep and consideration of the kinetics of a possible carrier transfer. *J Physiol*. 1951;

(118):23-39.

8. Jardetzky O. Simple allosteric model for membrane pumps. *Nature*. 1966; 211(5052):969-970. doi:10.1038/211969a0.

9. Hollenstein K, Dawson RJP, Locher KP. Structure and mechanism of ABC transporter proteins. *Curr Opin Struct Biol*. 2007; 17(4):412-418. doi:10.1016/j.sbi.2007.07.003.

10. Hvorup RN, Goetz B a, Niederer M, Hollenstein K, Perozo E, Locher KP. Asymmetry in the structure of the ABC transporter-binding protein complex BtuCD-BtuF. 2007; 317:1387-1390. doi:10.1126/science.1145950.

11. Oldham ML, Khare D, Quiocho FA, Davidson AL, Chen J. Crystal structure of a catalytic intermediate of the maltose transporter. *Nature*. 2007; 450:515-522. doi:10.1038/nature06264.

12. Oldham ML, Chen J. Crystal Structure of the Maltose Transporter in a Pretranslocation Intermediate State. *Science*. 2011;1202(2011):1202-1205. doi:10.1126/science.1200767.

13. Korkhov VM, Mireku S a, Locher KP. Structure of AMP-PNP-bound vitamin B12 transporter BtuCD-F. *Nature*. 2012; 490(7420):367-372. doi:10.1038/nature11442.

14. Oldham ML, Chen S, Chen J. Structural basis for substrate specificity in the *Escherichia coli* maltose transport system. *Proc Natl Acad Sci U S A*. 2013; 110(45):18132-18137. doi:10.1073/pnas.1311407110.

15. Bao H, Duong F. Discovery of an auto-regulation mechanism for the maltose ABC transporter MalFGK2. *PLoS One*. 2012; 7(4):e34836. doi:10.1371/journal.pone.0034836.

16. Goudsmits JMH, Jan Slotboom D, van Oijen AM. Single-molecule visualization of conformational changes and substrate transport in the vitamin B12 ABC importer BtuCD-F. *Nat Commun*. 2017; 8(1):1652. doi:10.1038/s41467-017-01815-7.

17. Kadaba NS, Kaiser JT, Johnson E, Lee A, Rees DC. The high affinity *E. coli* methionine ABC transporter: structure and allosteric regulation. *Science*. 2008; 321(5886):250-253. doi:10.1126/science.1157987.

18. Johnson E, Nguyen PT, Yeates TO, Rees DC. Inward facing conformations of the MetNI methionine ABC transporter: Implications for the mechanism of transinhibition. *Protein Sci*. 2012; 21(1):84-96. doi:10.1002/pro.765.

19. Yang JG, Rees DC. The Allosteric Regulatory Mechanism of the *Escherichia coli* MetNI Methionine ATP Binding Cassette (ABC) Transporter. *J Biol Chem*. 2015; 290(14):9135-9140. doi:10.1074/jbc.M114.603365.

20. Kadner RJ. Regulation of methionine transport activity in *Escherichia coli*. *J Bacteriol*. 1975; 122(1):110-119.

21. Lewinson O, Lee AT, Locher KP, Rees DC. A distinct mechanism for the ABC transporter BtuCD – BtuF revealed by the dynamics of complex formation. *Nat. Struct. Mol. Biol*. 2010; 17(3):332-338. doi:10.1038/nsmb.1770.

22. Nguyen PT, Li QW, Kadaba NS, Lai JY, Yang JG, Rees DC. The contribution of methionine to the stability of the *Escherichia coli* MetNIQ ABC transporter-substrate binding protein complex. *Biol Chem*. 2015; 396(9-10):1127-1134. doi:10.1515/hsz-2015-0131.

23. Kadner RJ, Watson WJ. Methionine Transport in *Escherichia coli* : Physiological and Genetic Evidence for Two Uptake Systems. *J Bacteriol*. 1974; 119(2):401-409.

24. Kadner RJ. Transport and utilization of D-methionine and other methionine sources in Escherichia coli. *J Bacteriol*. 1977; 129(1):207-216.

25. Studier FW. Protein production by auto-induction in high density shaking cultures. *Protein Expr Purif*. 2005; 41(1):207-234. doi:10.1016/j.pep.2005.01.016.

26. Strong M, Sawaya MR, Wang S, Phillips M, Cascio D, Eisenberg D. Toward the structural genomics of complexes: Crystal structure of a PE/PPE protein complex from *Mycobacterium tuberculosis*. *Proc Natl Acad Sci*. 2006; 103(21):8060-8065. doi:10.1073/pnas.0602606103.

27. Adams PD, Grosse-Kunstleve RW, Hung LW, et al. PHENIX: Building new software for automated crystallographic structure determination. *Acta Crystallogr Sect D Biol Crystallogr*. 2002;58(11):1948-1954. doi:10.1107/S0907444902016657.

28. Dimaio F, Echols N, Headd JJ, Terwilliger TC, Adams PD, Baker D. Improved low-resolution crystallographic refinement with Phenix and Rosetta. *Nat Methods*. 2013; 10(11):1102-1106. doi:10.1038/nmeth.2648.

29. Collaborative Computational Project N 4. The CCP4 suite: programs for protein crystallography. *Acta Crystallogr D Biol Crystallogr*. 1994; 50:760-763. doi:10.1107/S0907444994003112.

30. Emsley P, Cowtan K. Coot: Model-building tools for molecular graphics. *Acta Crystallogr Sect D Biol Crystallogr*. 2004; 60:2126-2132. doi:10.1107/S0907444904019158.

31. Gouridis G, Schuurman-wolters GK, Ploetz E, et al. Conformational dynamics in substrate-binding domains influences transport in the ABC importer GlnPQ. 2015;

22(1). doi:10.1038/nsmb.2929.

CHAPTER 4: CONCLUSION

I would like to use this chapter to summarize our key findings by answering the questions that I raised in Chapter 1.

(1) How does the binding protein interact with its transporter?

MetNI acquires ATP from the cytoplasm to form ATP-loaded MetNI, which binds apo MetQ to form the MetNIQ complex with a dissociation constant measured to be 27 nM. As shown in this thesis, in the complex, MetQ docks to the transmembrane subunits to form a substrate translocation pathway opened to the periplasm (Fig 4.1)

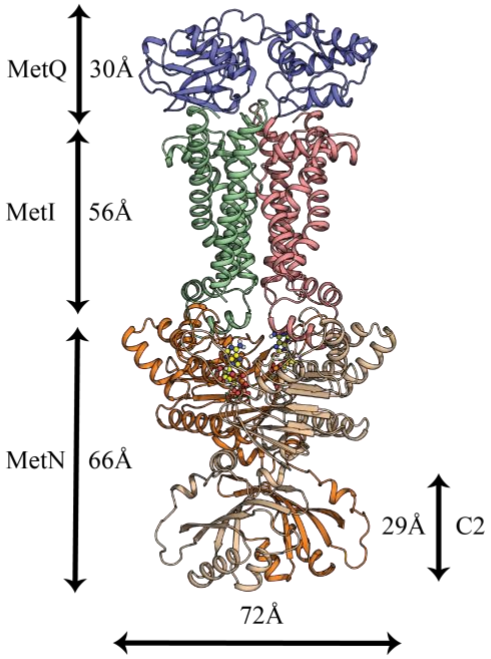

Figure 4.1. 2.95Å resolution crystal structure of the MetNIQ complex

(2) How does the C-regulatory domains regulate transport of methionine?

In an L-methionine-bound, IWF/inhibited conformation [18], an L-methionine substrate from one C2 domain forms hydrogen bonds with the other substrate at the interface β-sheet, stabilizing the inward-facing conformation of the transporter (Fig4b). In contrast, the OWF configuration shows a repositioning of the C2 domains by a register shift of the hydrogen bonding network between the two intermolecular β-sheets (A299 – A299 in the IWF to A299 – M301 in the OWF) (Fig4.2). This flexibility of the linkers between the NBDs and the C2 domains accomodates the dimerization of MetN subunits in the presence of ATP, and in the absence of L-methionine. In the presence of L-methionine, this rearrangement apparently cannot occur.

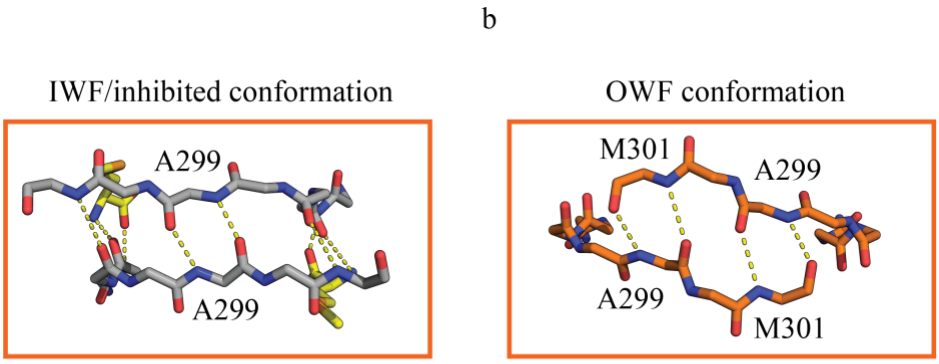

Fig 4.2. Structural insights of transport regulation by transinhibition

Top-down view of the C2 domains of the outward-facing conformation MetNIQ (OWF conformation) reveals shifts in hydrogen-bonding network (yellow dashes) A299 – M301, compared to that of the inward-facing conformation MetNI (IWF/inhibited conformation), A299 – A299 between 2 β-sheets (shown in ball-and-stick representations) at the domains'

interface. Binding of L-methionine at the C2 domains stabilizes the A299 – A299 hydrogen bond, and consequently locks the MetNI in its inward-facing conformation (PDB: 3TUZ).

(3) How does the binding protein bind or release its substrate?

A 42° hinge-type rotation of one lobe of MetQ to the other reorient four aromatic-ring residues to form a cage that select for methionine (Fig 4.3). The methionine substrate is also stabilized in the binding pocket by making hydrogen bond with the neighboring residues, including N229A, at its amino and carboxyl groups (Fig 4.3).

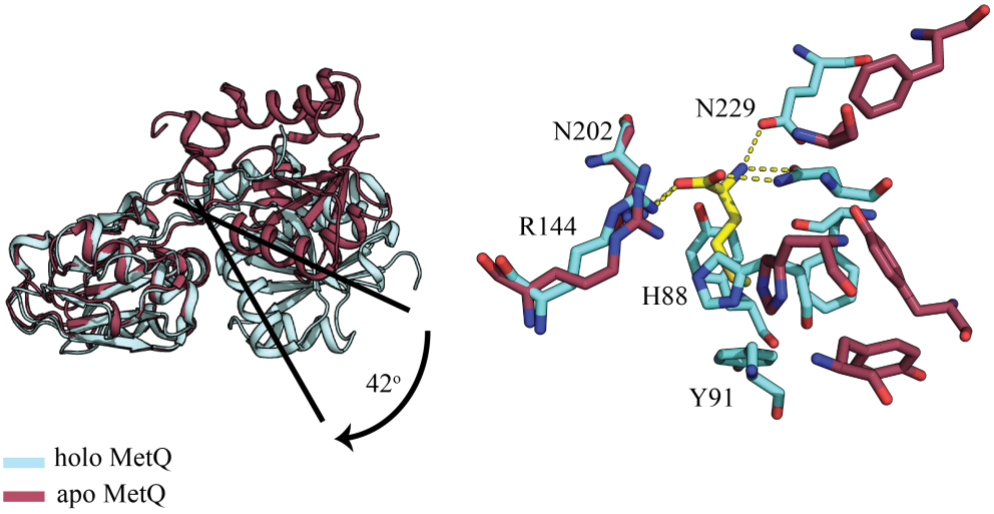

Figure 4.3. Binding of L-methionine substrate by MetQ at an atomic resolution

(4) What is the sequential order of interactions among the MetQ binding protein, the MetNI transporter, ATP and methionine?

In the presence of 1mM ATP in the cytoplasm, MetNI is quickly loaded with ATP at a K_d ~ 33μM. This ATP-loaded MetNI has high affinity (K_d ~ 0.027μM) toward the unliganded MetQ (apo MetQ) to form a stable complex. The whole MetNIQ assembly then binds to D-met or D-Semet, K_d ~ 6μM.

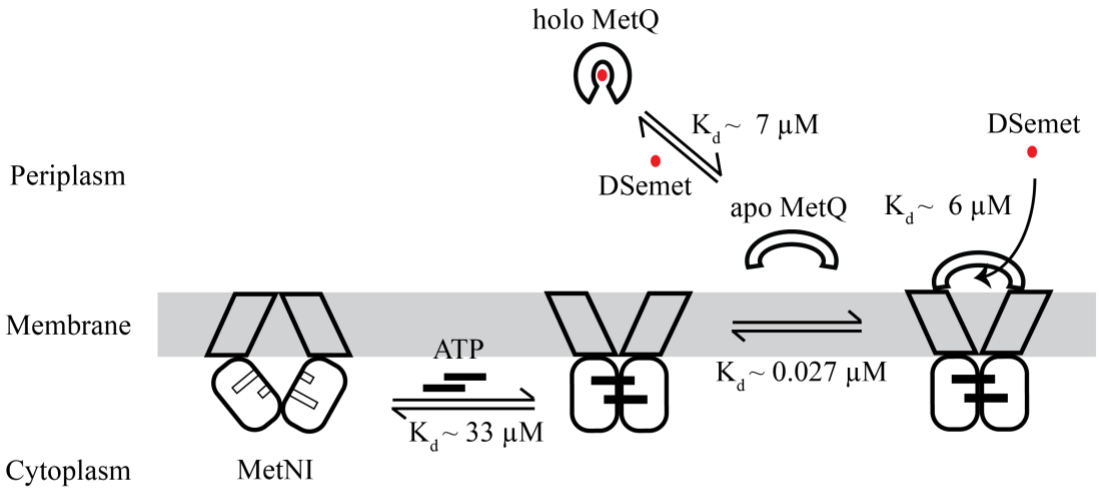

Figure 4.4. Thermodynamic sequential binding events of the MetNI methionine transport system

(5) What is the mechanistic model for the MetNI methionine transporter?

Combining the structural insights with thermodynamic binding constants and enzyme kinetic transport activities, we propose a mechanistic model to explain the biochemical and structural observations for the methionine transporter. A transport cycle starts with a resting- state MetNI that can bind two ATPs and acquire the outward-facing conformation MetNI (hypothetical model) (state 2). This hypothetical ATP-bound MetNI conformation was modeled based on knowledge of high basal ATPase activity of detergent-solubilized MetNI. The ATP-bound MetNI can associate with the apo MetQ to form a stable MetNIQ complex (reported here) (state 3). We propose that methionine can be loaded into the open translocation pathway. Gating residues, including Y160, F103, and M107, may function as a selectivity filter to ensure the right substrate in the cavity. Upon ATP hydrolysis, the translocation pathway opens towards the cytoplasm and releases methionine inside the cell (state 4). The transporter resets for the next cycle, unless internal L-methionine accumulates to a high concentration in the cell. L-methionine molecules then bind and lock the C2 domains by stabilizing the A299 –A299 hydrogen bonding networks at the C2 domains' interface, and, in turn, arrest MetNI in its IWF (PDB: 3TUZ) (state 5). This mechanistic model can be applied for other Type-I ABC homo-dimeric importers and for other ABC transporters subjected to trans-inhibition.

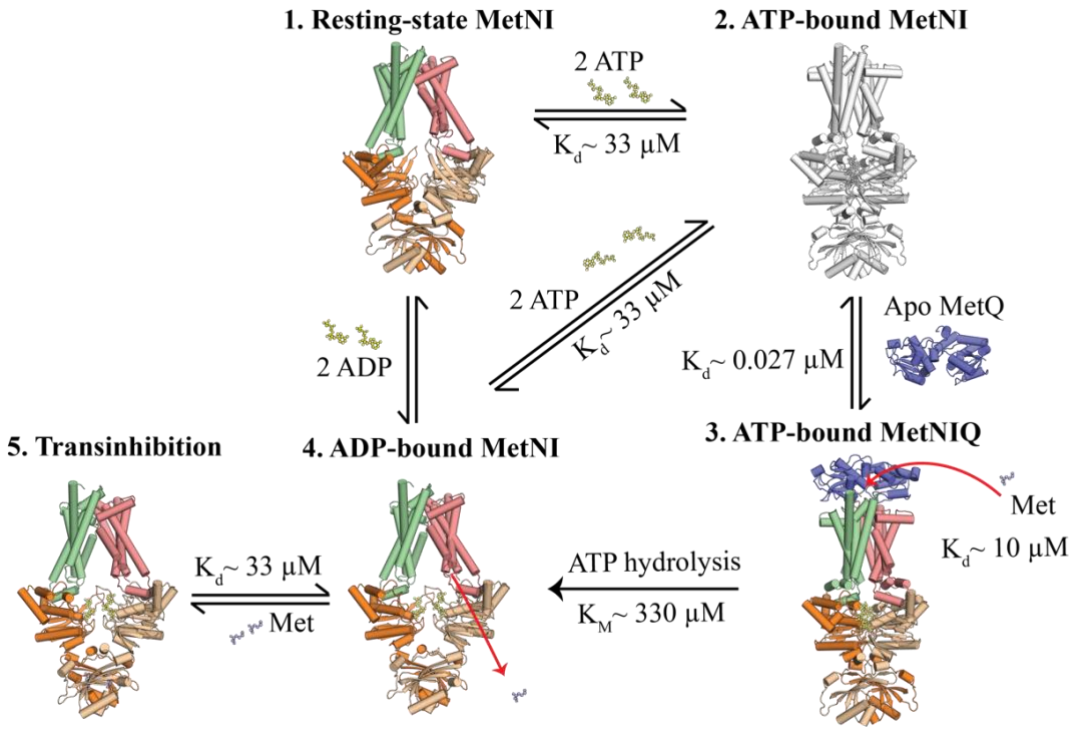

Figure 4.5. Proposed mechanistic atomic model of the methionine transporter